The G-alpha Gpa1 directs septin localization in the mating projection of *Saccharomyces cerevisiae* through its Ubiquitination Domain and Endocytic Machinery

Cory P. Johnson[1], Andrew Hart[2], Katherine F. Jarvis[2,4], Sarah G. Latario[2], Sudati Shrestha[2], Nicholas Leclerc[2], André Khalil[1,3,4], Joshua B. Kelley[1,2*]

[1]Graduate School of Biomedical Science and Engineering, University of Maine, Orono, ME

[2]Department of Molecular and Biomedical Sciences, University of Maine, Orono, ME

[3]Department of Chemical and Biomedical Engineering, University of Maine, Orono, ME

[4]CompuMAINE Laboratory University of Maine, Orono, ME

*Corresponding Author

joshua.b.kelley@maine.edu

5735 Hitchner Hall, University of Maine, Orono, ME

Keywords: Saccharomyces cerevisiae, yeast, pheromone, septins, polarity, g-alpha, g-protein, endocytosis, epsin, GPCR, Cdc42, GAP

Abstract

The yeast mating response uses a G-protein coupled receptor (GPCR), Ste2, to detect mating pheromone and initiate mating projection morphogenesis. The septin cytoskeleton plays a key role in the formation of the mating projection, forming structures at the base of the projection. Desensitization of the Gα, Gpa1, by the Regulator of G-protein Signaling (RGS), Sst2, is required for proper septin organization and morphogenesis. In cells where the Gα is hyperactive, septins are mislocalized to the site of polarity, and the cells are unable to track a pheromone gradient. We set out to identify the proteins that mediate Gα control of septins during the *Saccharomyces cerevisiae* mating response by making mutations to rescue septin localization in cells expressing the hyperactive Gα mutant *gpa1*^{G302S}. We found that single deletions of the septin chaperone Gic1, the Cdc42 GAP Bem3, and the epsins Ent1 and Ent2 rescued the polar cap accumulation of septins in the hyperactive Gα. We created an agent-based model of vesicle trafficking that predicts how changes in endocytic cargo licensing alters localization of endocytosis that mirrors the septin localization we see experimentally. We hypothesized that hyperactive Gα may increase the rate of endocytosis of a pheromone responsive cargo, thereby altering where septins are localized. Both the GPCR and the Gα are known to be internalized by clathrin-mediated endocytosis during the pheromone response. Deletion of the GPCR C-terminus to block internalization partially rescued septin organization. However, deletion of the Gpa1 ubiquitination domain required for its endocytosis completely abrogated septin accumulation at the polarity site. Our data support a model where the location of endocytosis serves as a spatial mark for septin structure assembly and that

desensitization of the Gα delays its endocytosis sufficiently that septins are placed peripheral to the site of Cdc42 polarity.

Abbreviations

Introduction

The *Saccharomyces cerevisiae* mating response is driven by a G-protein coupled receptor (GPCR) signaling pathway that initiates transcription of mating genes, polarization of the actin cytoskeleton and growth of a mating projection. Mating projection morphogenesis is dependent on septins, which are cytoskeletal filaments most famously known for their role in formation of the bud neck (Bridges and Gladfelter, 2015; McMurray et al., 2011). At a high dose of pheromone, as when close to a mate, yeast form a tight mating projection called a shmoo that is bounded by septins at the base (Giot and Konopka, 1997; Longtine et al., 1998). At an intermediate dose of pheromone, as when farther from a mate, the yeast undergo elongated growth towards the source of pheromone in a gradient tracking process that requires septins to control direction of growth (Kelley et al., 2015; Segall, 1993).

The α-Factor pheromone is detected by the GPCR Ste2, which initiates signaling through the heterotrimeric G-protein comprised of the α (Gpa1), β (Ste4), and γ (Ste18) subunits(Alvaro and Thorner, 2016). While Gβγ signaling has traditionally taken center stage for its regulation of both Cdc42-mediated polarity and MAPK signaling, Gα also controls downstream signaling. Gpa1 serves as a scaffold for the MAPK, Fus3, and through this role promotes the phosphorylation and activation of the formin Bni1 (Matheos et al., 2004; Metodiev et al., 2002). Active Gpa1 traffics to the endosome through its unique Ubiquitination Domain, a 109 amino acid insertion not found outside of fungi, and once at the endosome, Gpa1 interacts with the PI3 Kinase Vps34, promoting PI(3)P production (Dixit et al., 2014a; Slessareva and Dohlman, 2006). We previously found that Gpa1 activity influences the spatial distribution of septins during

the pheromone response and that septins are required for gradient tracking (Kelley et al., 2015).

Septins are evolutionarily conserved dynamic cytoskeletal filaments that are known for their roles as diffusion barriers, cortical actin regulators, and scaffolds that fortify membrane shape (Spiliotis and McMurray, 2020). During the yeast pheromone response, septin filaments form at the base of the mating projection, where they serve as scaffolds for signaling and promote morphogenesis and gradient tracking (Bharucha et al., 2008; Changwei et al., 2007; Gladfelter et al., 2005; Kelley et al., 2015). Septin deposition is controlled by the interplay of several Cdc42 effectors including the Rho-family member Cdc42, the Cdc42-binding septin chaperones called GTPase interactive components (Gic1 and Gic2), and the Cdc42 GTPase Activating Proteins (GAPs, Rga1, Rga2, and Bem3) (Khan et al., 2015). The Cdc42 GAPs also interact with the epsins Ent1 and Ent2, endocytic adaptor proteins that have also been shown to impact septin function (Aguilar et al., 2006).

The mechanism that controls the spatial distribution of septins during the pheromone response has not yet been elucidated, but we have previously found that Gpa1 desensitization is required for the normal localization of septins to the base of the mating projection (Kelley et al 2015). Gpa1 is desensitized through the actions of the regulator of G-protein signaling (RGS), Sst2, which serves as a GAP for Gpa1 (Apanovitch et al., 1998; Dohlman et al., 1996). Either deletion of the RGS or mutation of the Gα to disrupt RGS binding (*gpa1*^{G302S}) leads to septin mislocalization to the site of polarity (DiBello et al., 1998; Kelley et al., 2015). These septin changes result in a loss

of gradient tracking ability and defects in mating projection morphogenesis (Kelley et al., 2015).

Here, we have implemented a plan to uncover the pathway that Gpa1 uses to influence septin regulation. Using microfluidics and live-cell fluorescence microscopy, we looked for gene deletions that would restore peripheral septin distribution in cells expressing the hyperactive Gα mutant, *gpa1*^{G302S}. We found that Gpa1 control of septin distribution during the pheromone response is mediated by an Epsin-Bem3-Gic1 signaling axis. We developed a mathematical model that shows that endocytic events could generate the patterning that we see with septins. Following this, we disrupted endocytosis of both the receptor Ste2 and the Gα Gpa1, and found that, while both contribute to septin organization, Gpa1 endocytosis plays a larger role. Thus, the ubiquitination domain of Gpa1, which is required for its endocytosis, drives pheromone-induced septin organization.

Methods

Yeast Strains

Strains used in this study are listed in Table S1. All strains were constructed in the MATa haploid Saccharomyces cerevisiae parent strain, BY4741. All plasmids used in this study are included in Table S2. Polar cap (Bem1) and septin (Cdc3) proteins were tagged with GFP (Huh et al., 2003) and mCherry, respectively, at the native chromosomal locus through oligonucleotide-directed homologous recombination using primers listed in Table S3.

Cells were grown in rich medium (YPD) or synthetic medium (SC) at 30°C unless otherwise indicated. PCR products were transformed into parent yeast strains using standard lithium acetate transformation (Burke et al., 2000). Individual colonies were isolated by growth on standard selective media (SC leu-, SC ura-, SC his-, or YPD G418+). Transformants were verified using fluorescence microscopy, sequencing, and/or PCR.

Cloning

gpa1$^{\Delta UD\text{-}G302S}$ Plasmid Cloning The gpa1$^{\Delta UD\text{-}G302S}$ plasmid was constructed using the previously published pRS406-GPA1_truncΔUD (dixit et al 2014), which we received as a gift from the Dohlman Lab. We mutagenized the pRS406-GPA1_truncΔUD using the site-directed mutagenesis kit (NEB) in combination with the primers AHM-14 and AHM-15 listed in table 3. The plasmid was sequenced via PlasmidSaurus (https://www.plasmidsaurus.com/) to confirm successful mutagenesis of the glycine at position 302 to serine. Following sequence confirmation, we linearized the plasmid for genomic integration using AflII (NEB), a silent mutation inserted previously.

Gal-inducible Ste5-CTM Cloning. A galactose-inducible STE5 with the C-terminal membrane domain (CTM) of SNC2 was excised from the parent plasmid pGS5-CTM using *SacI-HF* and *ApaI* endonucleases. A pRSII416 plasmid (Chee and Haase, 2012) was linearized using the same enzymes, followed by a treatment of Antarctic phosphatase (New England Biolabs) to produce a new parent vector for the Gal-inducible Ste5-CTM fragment. Verification of the fragment and vector was performed using gel electrophoresis with a 0.8% TBE-agarose gel to confirm the size of the two products. The fragment and vector were then ligated together overnight at 16 °C using

T4 DNA ligase. The ligation mixture was transformed into DH5α competent *E. coli* cells (NEB #C2987), and colonies were isolated by growth on LB agar plates supplemented with 0.1 mg/mL carbenicillin. Plasmids were extracted from these transformants and were verified by restriction digest with *SacI-HF* and *ApaI*, followed by gel electrophoresis.

Microfluidics Experiments

Microfluidic devices were made by mixing SYLGARD 184 silicone polymer at 10(part A):1(part B) and poured directly onto a microfluidics device mold (Suzuki et al., 2021) that was fabricated by the University of Maine Frontier Institute for Research in Sensor Technologies (FIRST, https://umaine.edu/first/). Microfluidic chambers were made as previously described (Suzuki et al., 2021) Molds and coverslips were exposed to oxygen plasma for 50 seconds in a Harrick Plasma Cleaner PDC32G (Harrick Plasma) followed by fusion of the device mold to the coverslip. After fusing, the device was then baked in an oven at 80°C for at least 20 minutes to facilitate fusion of the mold to the coverslip.

Cultures were grown in 0.45µm-filtered Synthetic Complete + Dextrose to an OD600 between 0.1-0.8 at 30°C. Live-cell microfluidics experiments were performed using an IX83 (Olympus, Waltham MA) microscope and a Prime 95B CMOS Camera (Photometrics) controlled by Cell Sens 1.17 (Olympus). Fluorescence and Differential Interference Contrast (DIC) images were acquired using an Olympus-APON-60X-TIRF objective. Z-stacks of GFP and mCherry images were acquired using an X-Cite 120 LEDBoost (Excelitas). Cells were imaged in a “Dial-a-wave” based microfluidic device

that allowed for rapid switching of media while yeast remained in place (Bennet et al., 2011; Dixit et al., 2014b; Suzuki et al., 2021). Pheromone-containing media was verified using AlexaFluor 647 dye at 1:8000 dilution (Life Technologies) and imaged in a single plane. Cells were imaged at 20-minute intervals for 12 hours in Synthetic Complete media containing Dextrose (SCD) with 300nM pheromone present in the media. Imaging settings were determined based on experimental needs and were replicated for repeat experiments.

Ste5-CTM Experiments

Yeast cultures containing the Ste5-CTM (pRSII416) plasmid were diluted and grown overnight at 30 °C shaking in SC ura- media such that they did not exceed a saturating concentration (OD600 = 0.8). These cultures were then diluted to OD600 = 0.2, treated with either 0.5% galactose or 0.5% galactose and 10µM pheromone, and allowed to incubate for 4 hours shaking at 30 °C prior to imaging. Fluorescence microscopy was used to image Bem1-GFP and Cdc3-mCherry.

Image Analysis

Images were deconvolved using Huygens Software (Scientific Volume Imaging, Hilversum, Netherlands). For all fluorescent images, deconvolution was carried out with a theoretical point-spread function, 5 signal-to-noise ratio (GFP images) or 7 signal-to-noise ratio (mCherry images), maximum 500 iterations, and a quality change threshold of 0.01 using the classical algorithm. All other settings were set to default. Images were saved as 16-bit TIFF with linked-scale. Masks of fluorescent signal were created using a merged 8-bit RGB version of GFP and mCherry channels in FIJI and final segmentation was done prior to septin localization analysis in MATLAB. All septin localization analysis

was conducted using *whole_cell_cap_v4.m* for cell tracking and *combokeeper_v3.m* for line scan analysis Septin data was aligned to the polar cap profile using the regalignraw.m script (GitHub) and subsequently normalized to the fraction of total signal, as previously described (Kelley et al., 2015; Simke et al., 2022). Data was normalized to sum to 1 and 95% confidence intervals of the mean intensity were determined by bootstrapping. The referenced MATLAB scripts for these analyses are available on Github (https://github.com/Kelley-Lab-Computational-Biology/Spatial-Normalization).

Agent-Based Model Description

The agent-based model of cargo and vesicle transport was made using MATLAB (Mathworks). The code is available on Github at https://github.com/Kelley-Lab-Computational-Biology/Trafficking-Model. The membrane consists of 100 bins, each 0.1 µm wide. The model has a time step of 0.01 seconds, and we ran the model for 200,000 steps per simulation.

-*Agents:* Individual cargo is tracked and can become phosphorylated with a probability of 5e-5 per time step (termed 1x phosphorylation). Phosphorylated cargo can be ubiquitinated, which happens with a probability of 0.01 per time step. Cargo which is phosphorylated and ubiquitinated is now competent for endocytosis. If it diffuses into an endocytic pit, it will be trapped and will no longer diffuse.

-*Diffusion:* The system is scaled such that diffusion can happen one bin at a time and recapitulate realistic receptor diffusion rates (Valdez-Taubas and Pelham, 2003). Movement probability incorporates cargo concentration in adjacent bins to weight

diffusion probability to be more likely to move down the concentration gradient, as described previously (Azimi et al., 2011). The base probability to move one bin is 0.0024 per time step.

-*Vesicle Trafficking:* Exocytosis frequency has been measured by membrane capacitance at 2.4 events per minute in yeast that have been spheroplasted (Carrillo et al., 2015), and estimated to be 24 events per minute from microscopy data (Layton et al., 2011; Marco et al., 2007). Based on these two values, we chose an intermediate value of 8 events per minute, as yeast protoplasts may be experiencing cell wall stress that could decrease exocytosis. Endocytosis is set to happen at twice the rate of exocytosis with a single 2 bin exocytic event and 2 independent single bin endocytic events. These rates and sizes are balanced to roughly maintain membrane size. Exocytic events push the surrounding bins away from the site of exocytosis, while endocytic events remove the bin affected, bringing the surrounding bins next to each other. Location of exocytic events is determined by a probability distribution based on the Bem1 and Exo84 distributions calculated during the pheromone response previously (Brennwald, 2013; Kelley et al., 2015). We used the probability distribution equal to $[\text{Bem1}]^2 \times [\text{Exo84}]$ to account for the role of Cdc42-GTP in both directing actin organization and promoting vesicle fusion. Location of endocytic events is determined by selecting the most mature endocytic pit. Whenever an endocytic pit is removed, a new one is formed at the site of the highest ubiquitinated cargo, consistent with the finding that the presence of cargo regulates endocytic pit location (Pedersen et al., 2020).

Results

A scheme to identify proteins responsible for Gpa1 control of septins

We previously found that septin organization at the periphery of the polarity site in the yeast mating projection is dependent on the ability of the RGS, Sst2, to stimulate Gpa1 hydrolysis of GTP (Kelley et al., 2015). Here we set out to discover the signaling process that leads from active Gpa1 to control of septins. Our strategy was to delete genes involved in septin regulation (Figure 1A) from cells expressing either WT Gpa1 or the hyperactive gpa1^{G302S} mutant that is defective for binding to Sst2. Each strain has the Cdc42 scaffolding protein Bem1 tagged with GFP as a polar cap marker and the septin Cdc3 tagged with mCherry as a marker for septins. We then assessed these deletion strains for the ability to restore septin localization to the periphery of the polar cap. In cells responding to pheromone, septins form structures at the base of the mating projection, peripheral to the collection of polarity machinery that contains Cdc42 and Bem1 and is collectively known as the polar cap (Figure 1B). To map our baseline septin profiles we used live-cell fluorescence microscopy and computational image analysis of Bem1-GFP and Cdc3-mCherry. We collected high-quality images at single time-points to visualize discrete septin structures (Figure 1B). However, because septin structures change through the pheromone response, we used live-cell microscopy in a microfluidic device to monitor the polar cap and septins through 12 hours of pheromone response using a flat dose of 300nM pheromone, which is sufficient to stimulate shmoo formation and prevent sustained elongation (Figure 1C and D) (Kelley et al., 2015).

To quantify the average distribution of septins along the periphery of the cell, we spatially normalized our septin profiles to the center of the polar cap – indicated by peak

fluorescence of Bem1-GFP, a Cdc42-GTP binding protein, as we have done previously (Kelley et al., 2015; Simke et al., 2022). We averaged the spatially normalized septin profiles across time points and cells to yield an average septin distribution for each strain. We then bootstrapped 95% confidence intervals (indicated by shaded regions): non-overlapping confidence intervals indicate statistically significant differences in septin distribution for $p < 0.05$. Our metric for septin rescue is shifting the septin distributions in the hyperactive *gpa1*^{G302S} cells back toward the septin shape in WT cells (Figure 1E).

Gpa1 regulation of septins occurs in addition to a default septin regulation pathway in response to pheromone.

Septins are organized into a ring structure during mitosis in haploids, where Gpa1 levels are high, and in diploids, where Gpa1 levels are much lower (de Godoy et al., 2008). We would anticipate that mechanisms for septin organization during cell division are independent of Gpa1, however, we do not know if Gpa1 is required for septin organization during the pheromone response. We tested whether Gpa1 activity is required for septin organization during the pheromone response by initializing MAPK signaling and Cdc42-mediated polarity by using a mutant MAPK scaffold, Ste5, modified on its C-terminus to contain a transmembrane domain (Ste5-CTM) (Pryciak and Huntress, 1998). Expression is controlled by a GAL promoter such that the pheromone pathway is inducible by galactose, without activation of the receptor Ste2, or activation of the hetero-trimeric G-protein, Gpa1, Ste4, and Ste18. We grew cells in raffinose and then treated with either 0.5% galactose for 4 hours, or 0.5% galactose and 10 µM pheromone for 4 hours, and imaged Bem1-GFP and Cdc3-mCherry. Cells were able to

place septin structures at the base of the mating projection in the presence of galactose alone, or with both galactose and pheromone (Figure 1F). When we quantified the average location of septins in this experiment (Figure 1G), we find that in both treatments, the average distribution is moderately flat, suggesting that the spatial placement of septins is more random than in cells that are not expressing Ste5-CTM. Thus, Gpa1 activation is not required for septin structures to be formed during the pheromone response, indicating that Gpa1 control of septins is layered on top of normal septin regulatory machinery.

Gic1, but not Gic2, contributes to Gpa1-driven septin organization

The Cdc42-interacting paralogs, Gic1 and Gic2, are Cdc42-GTP binding proteins involved in the recruitment of septins to the polarity site during mitotic budding and in septin bundling activity *in vitro* (Figure 2A) (Iwase et al., 2006; Sadian et al., 2013). We constructed single-gene-deletions of Gic1 and Gic2 from yeast expressing hyperactive *gpa1*^{G302S} and examined the polar cap (Bem1-GFP) and septin (Cdc3-mCherry) distribution (Figure 2B, C, D). High resolution, single time point images reveal that hyperactive *gpa1*^{G302S} cells lacking Gic1 placed septin structures further from the polar cap compared to cells lacking Gic2 (Figure 2B). We found through live-cell imaging (as conducted above) that cell morphology and septin distribution in hyperactive *gpa1*^{G302S} cells lacking Gic1 resembled WT-like phenotypes (Figure 2C). This observation was supported by septin distribution quantification performed as above (Figure 2E). Thus, Gic1 has a role in septin organization during the pheromone response distinct from that of Gic2 and is required for Gpa1 control of septins.

The Cdc42GAP, Bem3, mediates Gpa1 control of septin structures

Cdc42 GAP activity promotes septin structure assembly on the plasma membrane (Figure 3A) (Gladfelter et al., 2002; Khan et al., 2015). Yeast express three Cdc42 GAPs: Rga1, Rga2, and Bem3 (Smith et al., 2002). At high resolution we found that all three single-gene deletions in hyperactive *gpa1*^{G302S} mutants had at least some overlap between septins and the polar cap, and at the same time all three mutants had septin structures set up far from the polar cap as well (Figure 3B). However, live-cell microscopy at lower pheromone dose revealed that cells expressing hyperactive gpa*1*^{G302S} and lacking Bem3 displayed more definitive separation between septins and the polar cap compared to mutants lacking Rga1 or Rga2 (Figure 3C-E). When we quantitatively examined the septin organization over time, we confirmed that hyperactive *gpa1*^{G302S} mutants lacking Bem3 robustly rescued septin distribution (Figure3F). We also found that hyperactive *gpa1*^{G302S} mutants lacking either Rga1 or Rga2 mildly rescued aberrant septin distribution (Figure 3F). Thus, while all three Cdc42 GAPS influence Gpa1 control of septins, Bem3 contributes more significantly than Rga1 or Rga2.

The endocytosis adaptors Ent1 and Ent2 direct Gpa1 dependent pheromone-induced septin organization

Cdc42 GAPs bind directly to the epsin endocytic-adaptor proteins, Ent1 and Ent2, in an interaction thought to couple Cdc42 regulation to endocytosis (Aguilar et al., 2006). Additionally, epsins are known to differentially contribute to septin organization during cell division (Mukherjee et al., 2009). We hypothesized that epsins may also contribute to septin organization during the pheromone response (Figure 4A). As previously described, we investigated septin organization in hyperactive *gpa1*^{G302S}

mutants lacking either Ent1 or Ent2 at high resolution (Figure 4B), via time course imaging (Figure 4C-D), and through time-averaged quantitation of peak septin distribution in relation to the polar cap (Figure 4E). At high resolution we found cells lacking Ent1 clearly rescued aberrant septin structures. Additionally, cells lacking Ent2 rescued the septin phenotype but with a pronounced peak of septins at the center of the polar cap (Figure 4B). Timelapse imaging also revealed the same phenotype found at high resolution (Figure 4C-D) and quantitation of peak septin distribution confirmed that single-gene deletion of either epsin robustly rescues aberrant septin distributions in hyperactive *gpa1*^{G302S} mutants (Figure 4E). Thus, both Ent1 and Ent2 are mediators of Gpa1 control of septin distribution during the pheromone response.

An agent-based model of vesicle trafficking shows that location of endocytosis could explain septin organization.

We have found that the endocytic adaptor protein Ent1 and Ent2 are both involved in the control of septin distribution by Gpa1. Furthermore, rescue of septin organization in each experiment has been through a loss of function (deletion) mutation, which should slow cellular processes in which these proteins are involved. Epsins are endocytic adapter proteins, which led us to hypothesize that endocytosis itself may be able to serve as a spatial mark for septin organization. In this scenario, changes in the rate that cargo becomes competent for endocytosis could give rise to the septin distribution changes that we see. To test this, we developed an agent-based stochastic model of protein trafficking. This model is described in Figure 5. Cargo is delivered to the membrane, diffuses, undergoes endocytosis, and is tracked spatially over time. Like the receptor, Ste2, it has a probability to become phosphorylated, and phosphorylated

cargo has a probability to become ubiquitinated and therefore competent for endocytosis (Figure 5A) (Lu et al., 2016). These reactions occur in a discretized 1 dimensional membrane that can grow and shrink with endo- and exocytosis (Figure 5B). The location of exocytosis is based upon the distributions of Bem1 and Exo84 that we have previously measured (Figure 5C) (Kelley et al., 2015). The number of endocytic pits is kept constant, such that when an endocytic pit is endocytosed, a new pit forms at a new site based upon the amount of ubiquitinated cargo, consistent with polarized endocytic cargo driving the polarization of endocytosis (Figure 6 D) (Pedersen et al., 2020). Diffusion within the membrane is carried out as described by Azimi et al, where the direction of diffusion is biased by the occupancy of the adjacent bins such that diffusion into bins with fewer molecules is more likely (Figure 5E) (Azimi et al., 2011). Ubiquitinated cargo that enters an endocytic pit becomes trapped there, and eventually will be internalized (Figure 6F). We performed simulations where we varied the rate of phosphorylation and examined the distribution of ubiquitinated cargo and the location of endocytic events.

To test the effects of increasing the rate of cargo endocytosis, we varied the rate of phosphorylation in our model, and ran multiple simulations with each condition. We simulated cargo location and modification on the surface of the cell over 30+ minutes in-model time (Figure 6A). Increasing the rate of phosphorylation from baseline (1x) 5-fold or 25-fold increases the fraction of endocytic events that occur at the center of the polar cap (Figure 6B, C). The increased phosphorylation rates mean that cargo cannot travel along the membrane as far before being internalized.

Altering the rate that cargo becomes competent for endocytosis allows us to qualitatively recreate the septin distributions we have measured in WT and *gpa1*^{G302S} strains at 300 nM. When we compare our simulation of endocytosis locations to our experimentally measured septin distributions, we see that the 1X phosphorylation simulation of endocytic events is similar to septin distribution in our WT cells treated with 300 nM pheromone. The simulations of endocytosis at a high rate of endocytic competency, the 25X phosphorylation rate, generate endocytic events with a distribution similar to septins in the hyperactive *gpa1*^{G302S} mutant strain (Figure 7A). Our model simulations suggest that a 5x higher rate of endocytosis competency would lead to endocytosis events closer to the polar cap than we had measured (Figure 7B). If our model is accurately recapitulating the system, then we would expect that the endocytic distribution of the 5X phosphorylation rate would predict the septin distribution in the presence of a high dose of pheromone. In this case, the pathway activity would be high, but the Gα would still be able to turn off. We treated WT cells with 10 µM pheromone for 2 hours and measured Cdc3-mCherry distribution relative to the polar cap (Figure 7B). The measured septin distribution matches the simulation remarkably well, even down to the same asymmetry in both simulated endocytic events and septin distribution, which we attribute to happy coincidence, as we have no reason to believe there is an underlying asymmetry in the biology and our model should not have any intrinsic asymmetry. These data do not necessarily mean that *gpa1*^{G302S} increases phosphorylation of a cargo *per se*, but it does suggest that increasing the rate that a cargo becomes competent for endocytosis and coupling that endocytic event to

assembly of macromolecular complexes of septin would be capable of creating the septin distributions we see in WT and *gpa1*^{G302S} mutants.

Endocytosis of Gα and the pheromone receptor directs pheromone-induced septin distribution

We have found that the endocytic adaptor proteins Ent1 and Ent2 are required for Gα control of septins and that our mathematical model can reconstruct the distribution of septin peaks seen in our experimental data by altering the rate that cargo become endocytically competent. These data raise the question: Can endocytic cargo(s) drive septin deposition during the pheromone response?

The pheromone receptor, Ste2, is both phosphorylated and ubiquitinated at its C-terminus to control its endocytosis (Dunn and Hicke, 2001; Hicke et al., 1998). We constructed cells lacking the receptor C-terminus from codon 326 (*ste2*$^{\Delta C}$), a critical region for control of receptor endocytosis (Konopka et al., 1988). We then investigated the effect of the *ste2*$^{\Delta C}$ on septin localization in cells expressing *gpa1*^{G302S}. We found that *gpa1*^{G302S} mutants lacking the C-terminus of Ste2 partially rescued the septin defect (Figure 8A,B). Morphologically, the *gpa1*^{G302S} *ste2*$^{\Delta C}$ double mutants are very round, with poor mating projection formation, consistent with septin defects. In contrast to this partial rescue, epsin deletions completely rescued the septin organization and restored elongated (albeit still abnormal) growth, suggesting there could be another cargo driving septin distribution.

Gpa1 contains a ubiquitination domain (UD) that promotes endocytosis and subsequent trafficking through the endomembrane system (Dixit et al., 2014a; Wang et

al., 2005a). We hypothesized that endocytosis of Gpa1 (via the UD) directs septin deposition. We constructed an integrating plasmid to replace the wildtype Gpa1 locus with a *gpa1*^{G302S} lacking the UD (*gpa1*$^{G302S\text{-}\Delta UD}$) and monitored both the polar cap and septins as we did in Figures 1-4 (Dixit et al., 2014a). Our single time point imaging of hyperactive mutants lacking the UD of Gpa1 showed rescue of the *gpa1*^{G302S}-induced septin defects, similar to the rescue seen in the *ste2*$^{\Delta C}$ (Figure 8A). The degree of rescue was more apparent in live-cell microscopy carried out under a more physiological pheromone dose of 300 nM in microfluidic devices (Figure 8C). Under these conditions, there is clear elongation of the cells, with septin structures well separated from the polar cap.

While the *gpa1*^{G302S} mutant leads to increased pathway sensitivity, the gpa1$^{\Delta UD}$ mutant is known to lead to decreased pathway sensitivity (DiBello et al., 1998; Wang et al., 2005b). It is noteworthy that cells expressing *gpa1*$^{G302S\text{-}\Delta UD}$ arrested in G1 for less time than WT cells. When these cells were exposed to 300nM pheromone – as all other strains were exposed to – we found that cells reverted to mitotic behavior after only 8 hours of pheromone exposure (Movie S1). Both WT and *gpa1*^{G302S} cells under these conditions will respond to pheromone for the entire 12 hours, indicating that the deletion of the UD is dominant to the gpa1^{G302S} reduction of RGS interaction, at least for arrest of the cell cycle. For the purposes of our septin experiments, we found that increasing the concentration of pheromone to 1µM lead to the *gpa1*$^{G302S\text{-}\Delta UD}$ cells continuing to develop mating projections for the full 12-hour time course (Movie S1). Additionally, we quantified septin distribution in the *gpa1*$^{G302S\text{-}\Delta UD}$ mutants at 300nM pheromone and

1μM pheromone and found that pheromone concentration did not affect septin distribution profiles during the pheromone response (Figure S1).

Finally, we quantified the septin distributions of cells expressing the hyperactive *gpa1*^{G302S} and lacking either the C-terminus of Ste2 (*gpa1*^{G302S} *ste2*$^{\Delta C}$) or the UD of Gpa1 (*gpa1*$^{G302S\text{-}\Delta UD}$) relative to the center of the polar cap as described above. We found that hyperactive cells lacking the C-terminus of Ste2 partially rescued the *gpa1*^{G302S}-induced septin defects, while cells lacking the Gpa1 UD fully rescued the septin defect in relation to the polar cap (Figure 8E). Disruption of endocytosis of Gpa1, and to a lesser degree, Ste2, must therefore slow septin structure formation in the *gpa1*^{G302S} mutant, allowing septins sufficient time to move to the periphery of the polarity site prior to forming higher-order structures. Thus, Gpa1 influences septin organization via protein domains required for endocytosis: the Gpa1 UD and the C-terminus of Ste2.

Discussion

Here we describe the mechanism for Gpa1 control of septins in the yeast pheromone response. We tested for rescue of septin organization by deletion of known components of the septin regulatory system, including the Cdc42 effectors Gic1 and Gic2, and the Cdc42-GAPs Rga1, Rga2, and Bem3. We found that pheromone-induced septin organization is dependent upon Gic1, but not its paralog Gic2 and preferentially uses the Cdc42 GAP Bem3. Because Cdc42 GAPs bind to the Ent1 and Ent2 endocytic adaptors, we examined the ability of epsin deletions to rescue Gpa1-induced septin defects. We found that Ent1 and Ent2 contribute equally to pheromone-induced septin organization. Based on Ent1/2 roles in endocytosis, we used an agent-based

mathematical model to test if the location of endocytic events could explain septin distribution. Our model recapitulates the wild type and mutant Gpa1-induced septin distributions when the following two assumptions are made: 1) that *gpa1*^{G302S} alters when a cargo is marked for clathrin-mediated endocytosis and 2) that endocytosis is spatially coupled to septin structure organization. Based on these results, we hypothesized that a pheromone-dependent endocytic cargo was responsible for Gpa1 control of septins. A likely candidate was the pheromone responsive GPCR, Ste2, which is known to undergo endocytosis in response to pheromone (Dores et al., 2010; Hicke and Riezman, 1996; Lu et al., 2016). However, when we disrupted Ste2 endocytosis, we only saw a moderate effect on septin organization. Gpa1 internalization is less well characterized but is known to be dependent upon its Ubiquitin Domain (UD) (Dixit et al., 2014a). Remarkably, blocking Gpa1 endocytosis by removal of the UD led to complete recovery of septins to the periphery of the polar cap in the presence of the hyperactive *gpa1*^{G302S} mutation.

Endocytosis of Cargo as a Marker for Septin Organization

Septin organization occurs during mitosis, with no Gα activity necessary, and we have shown that Gpa1 activity is dispensable for septin organization during the pheromone response, as initiating signaling with the MAPK scaffold, Ste5, leads to septin structure formation at the base of the mating projection. Thus, Gpa1 adds an additional layer of septin regulation on top of the normal process. Our data lead us to the following model (Figure 9): In the presence of pheromone, when Gpa1 and Ste2 are phosphorylated and then ubiquitinated, they recruit epsins and Cdc42 GAPs to the site of endocytosis. The recruitment of the Cdc42GAP promotes Cdc42 hydrolysis of GTP,

and subsequent organization of higher order septin structures in a Gic dependent manner. When Gpa1 is hyperactive, it becomes competent for endocytosis sooner, recruiting epsins and Cdc42 GAPs earlier, and driving septin organization closer to the polar cap.

Previous models of septin organization incorporated exocytosis as a driving force for clearance of septins from the bud site, and Cdc42 GAP function as the “timer” dictating how far septins were pushed before assembly into higher order structures (Okada et al., 2013). Our data add a new wrinkle to this, suggesting that epsin-mediated endocytosis may control *where* septins organize into higher order structures. Thus, vesicle trafficking drives the movement of septins away from the polar cap on the “conveyor belt” of the plasma membrane (moving away from exocytic events and towards endocytic events) (Figure 9B). Coupled to this, endocytosis provides the spatial cue that septins should transition from “passengers” on this conveyor belt to establishing higher-order structures at the site of clathrin mediated endocytosis.

Disruption of receptor endocytosis showed a partial rescue of septin, suggesting that endocytic cargoes, broadly, promote septin organization. But why does Gpa1 have a larger effect? Both receptor and Gα undergo clathrin-mediated endocytosis in response to pheromone, but Ste2 endocytosis is likely not linked to Gpa1 activation. So Ste2 recruitment of epsins and GAPs may be contributing to a fraction of septin organization as normal. As such, removal of the Ste2-contribution reduces some of the septin organization signaling happening close to the polar cap, but hyperactive Gpa1 continues to drive significant amounts of septin organization close to the polar cap.

Our model for Gα control of septins during the pheromone response predicts that the distance between the polar cap and septin structures would be smaller for high doses and get larger at lower doses. We found that septins accumulated closer to the polarity site at 10 uM than at 300nM (Figure 7B) and indeed, this is what we saw in our previous work (Kelley et al., 2015), where cells responding to an intermediate of pheromone dose (~75 nM, center of a 0-150 nM gradient) established septin structures farther from the center of the polar cap than cells exposed to a high dose of pheromone (300 nM pheromone). Our model couples pheromone dose to septin spatial regulation, which is necessary for a mechanistic understanding of gradient tracking.

Implications for gradient tracking

We previously found that cells without functional septins grow in a straight line, unable to correct their orientation by turning (Kelley et al., 2015). WT cells that turn have septins on the inside of the turn. Thus, asymmetric distribution of septins on the inside of the turn (up-gradient) appears to be required for error correction during gradient tracking (Kelley et al., 2015). Our findings that Gpa1 activity level influences septin organization through the endocytosis machinery provides a potential mechanism for asymmetric septin organization (Figure 9B). Simply, higher active Gpa1 on the upgradient side of the cell results in increased Gpa1 endocytosis. The endocytic machinery recruited to the site of endocytosis promotes septin organization on the up-gradient side of the cell. The accumulation of septins could then facilitate the turning of the cell. Future studies will be needed to address how activation of Gpa1 influences internalization through its UD.

Epsins and Cdc42-GAPs

These results raise the question of whether organization of the septin ring during mitosis is also controlled by endocytic events? The Aguilar lab has found that overexpression of the Epsin N-terminal Homology Domain from Ent2 (ENTH2) leads to defects in the organization of septins during mitosis (Mukherjee et al., 2009). Furthermore, they found that ENTH2 overexpression affects Bem3 localization. It may be that Epsin recruitment of Bem3 is broadly used to control septin organization.

The Bi and Goryachev labs showed that exocytosis serves to drive septin formation into a ring structure during mitosis, with the assumption that GAP activity would serve as the limit on expansion of the ring, resulting in septin organization at the edge of the polar cap (Okada et al., 2013). It may be that the initial cue to form septin structures during mitosis arises from endocytic cargoes recruiting Epsin/Bem3 complexes, and that further action by Rga1 and Rga2 bound to these new septin structures serves to reinforce structure formation. By contrast, Rga1 and Rga2 show little localization during the pheromone response (Kelley et al., 2015) so the bulk of the responsibility to control septins may fall to Bem3.

Gα endocytosis as a signaling event

Here, we show that Gpa1 influences septin organization through its UD, the yeast-specific domain required for Gpa1 endocytosis (Figure 8) (Dixit et al., 2014a; Wang et al., 2005b). While the Gpa1 UD is unique to yeast Gα, mammalian cells also endocytically regulate Gα via β-arrestins (Smith et al., 2021). Mammalian endocytosis of Gα occurs indirectly via receptor C-terminal interaction and not directly with the Gα subunit (Shenoy and Lefkowitz, 2003). Indeed, many components of clathrin mediated

endocytosis are conserved between yeast and mammalian cells: 1) mammalian epsins bind AP2 (Chen et al., 1998), 2) mammalian epsins bind Cdc42-GAP (Coon et al., 2010), and mammalian epsins maintain the ubiquitin interacting motif necessary for endocytic cargo binding (Wendland, 2002). Therefore, future research will need to examine whether mammalian cells may also utilize Gα endocytosis as a spatial landmark for septin organization during morphogenesis.

Acknowledgements

The authors wish to thank Holly Goodson and Melissa Maginnis for helpful discussions. The authors would also like to thank Niklas Hase, the Shmoo Crew and other former members of the Kelley Lab for experimental and logistical input including. This work was supported by the National Institutes of Health Grant R15-GM140409 to JBK.

Author Contributions

CPJ wrote the manuscript -original draft, review, and edits, visualization; designed, conducted, analyzed, and oversaw the experiments. AH wrote the manuscript -review and edits, collected, and analyzed data. KJF wrote the manuscript -original draft, review, and edits, designed and conducted experiments (mathematical modeling), and created software. SGL wrote the manuscript -review and edits, collected, and analyzed data. SS wrote the manuscript -review and edits, collected and analyzed data. NL wrote the manuscript -review and edits, collected and analyzed data. AK wrote the manuscript-review and edits, and contributed supervision. JBK wrote the manuscript -original draft, review and edits, visualization, designed experiments, acquired funding, contributed supervision, conceptualized and oversaw the project.

Figure Legends

Figure 1. Pheromone-induced septin accumulation occurs at the center of the polar cap in Hyper Gα mutants.

A) Schematic of key players in septin deposition in yeast. Cdc42-GTP binds to GICs, which are required for septin recruitment. GAP activity promotes Cdc42 hydrolysis of GTP to GDP and promotes septin structure formation. B) Representative images of pheromone treated yeast (2hrs with saturating pheromone) expressing endogenous Bem1-GFP (Polar Cap) and Cdc3-mCherry (Septin) in WT (top panels) and in the hyperactive Gα (*gpa1*^{G302S}) mutant (bottom panels). Scale bar represents 3µm and white arrows indicate sites of peripheral septin localization, while black arrow indicates septins localized close to the polar cap. C) Representative images of WT cells expressing endogenous Bem1-GFP (Polar Cap) and Cdc3-mCherry (Septin) exposed to 300 nM pheromone in a microfluidic chamber for 12hrs. Images of cells at 0min (top row), 360min (middle-row), and 720min (bottom row) are displayed with split-channel (left and middle columns) and merged images (right column). Arrows indicate septins organizes at the base of projections, away from the polar cap. Scale bar represents 5µm. D) Representative images of *gpa1*^{G302S} yeast expressing endogenous Bem1-GFP (Polar Cap) and Cdc3-mCherry (Septin) exposed to saturating pheromone in a microfluidic chamber for 12hrs. Images of cells at 0min (top row), 360min (middle-row), and 720min (bottom row) are displayed with split-channel (left and middle columns) and merged images (right column). Arrows indicate septins accumulating close to the polar cap. Scale bar represents 5µm. E) Time-averaged quantification of the fraction (y-axis)

of septin and its distribution relative to the polar cap (x-axis). Lines are representations of time-averaged data (37 time points; 20min intervals for 12hrs) and shaded regions surrounding lines are 95% confidence intervals. Lines are representative of two combined experiments (WT n = 51 cells and *gpa1*^{G302S} n = 73 cells). F) Representative images of cells expressing the GAL-inducible Ste5-CTM that activates the mating pathway without activation of Ste2, Gpa1, or Ste4/Ste18. Cells were treated with 0.5% galactose or 0.5% galactose & 10 µM pheromone for 4 hours. Arrows indicate sites of septin organization at the base of the mating projection. G) Quantitation of septin organization in cells expressing the GAL-inducible Ste5-CTM. Shaded area represents the 95% confidence intervals. n = 128 for +Gal and n = 139 for +Gal +Pheromone, across two separate experiments.

Figure 2. Gα control of septins is preferentially mediated by Gic1 rather than Gic2. A) Schematic shows that we predict decreased septin recruitment in individual genetic deletions of Gic1 or Gic2 in yeast with hyperactive Gα, *gpa1*^{G302S}. B) Representative images of pheromone treated yeast (2hrs with saturating pheromone) expressing endogenous Bem1-GFP (Polar Cap) and Cdc3-mCherry (Septin) in *gpa1*^{G302S} cells lacking Gic1 or Gic2. Scale bar represents 3µm and white arrows indicate sites of peripheral septin localization. C) Representative images of *gpa1*^{G302S}*-gic1Δ* cells expressing endogenous Bem1-GFP (Polar Cap) and Cdc3-mCherry (Septin) exposed to 300 nM pheromone in a microfluidic chamber for 12hrs. Images of cells at 0min (top row), 360min (middle row), and 720min (bottom row) are displayed with split-channel (left and middle columns) and merged images (right column). Scale bar represents 5µm. D) Representative images of *gpa1*^{G302S}*gic2Δ* yeast expressing endogenous Bem1-GFP (Polar Cap) and Cdc3-mCherry (Septin) exposed to 300 nM pheromone in a microfluidic chamber for 12hrs. Images of cells at 0min (top row), 360min (middle-row), and 720min (bottom row) are displayed with split-channel (left and middle columns) and merged images (right column). Scale bar represents 5µm. E) Time-averaged quantification of the fraction (y-axis) of septin distribution relative to the polar cap (x-axis). Lines are smoothed representations of time-averaged data (37 time points; 20min intervals for 12hrs) and shaded regions surrounding lines are 95% confidence intervals. Lines are representative of two combined experiments (*gpa1*^{G302S}*-gic1Δ* n = 63 cells and *gpa1*^{G302S}*-gic2Δ* n = 68 cells).

Figure 3. Gα control of septins is preferentially mediated by the Cdc42GAP Bem3, rather than Rga1 or Rga2.

A) Schematic representation of our predicted outcome for individual genetic deletion of the GAPs Rga1, Rga2, or Bem3 in *gpa1*^{G302S} yeast. We predicted the lack of individual Cdc42-GAPs would reduce septin recruitment to sites of polarity during the pheromone response and ultimately rescue the *gpa1*^{G302S} phenotype of early septin deposition (top-panel). B) Representative images of pheromone treated yeast (2hrs with saturating pheromone) at high magnification (200X prior to image cropping) expressing endogenous Bem1-GFP (Polar Cap) and Cdc3-mCherry (Septin) in *gpa1*^{G302S} cells lacking Rga1 (top row), Rga2 (middle row), or Bem3 (bottom row). Scale bar represents 3µm. Back arrows indicate sites of septin structure close to the polar cap and white arrows indicate sites of peripheral septin localization. C) Representative images of *gpa1*^{G302S}*-rga1Δ* cells expressing endogenous Bem1-GFP (Polar Cap) and Cdc3-mCherry (Septin) exposed to saturating pheromone in a microfluidic chamber for 12hrs. Images of cells at 0min (top row), 360min (middle-row), and 720min (bottom row) are displayed with split-channel (left and middle columns) and merged images (right column). Scale bar represents 5µm. D) Representative images of *gpa1*^{G302S}*-rga2Δ* yeast expressing endogenous Bem1-GFP (Polar Cap) and Cdc3-mCherry (Septin) exposed to saturating pheromone in a microfluidic chamber for 12hrs. Images of cells at 0min (top row), 360min (middle-row), and 720min (bottom row) are displayed with split-channel (left and middle columns) and merged images (right column). Scale bar represents 5µm. E) Representative images of *gpa1*^{G302S}*-bem3Δ* yeast expressing endogenous Bem1-GFP (Polar Cap) and Cdc3-mCherry (Septin) exposed to saturating

pheromone in a microfluidic chamber for 12hrs. Images of cells at 0min (top row), 360min (middle-row), and 720min (bottom row) are displayed with split-channel (left and middle columns) and merged images (right column). Scale bar represents 5µm. F) Time-averaged quantification of the fraction (y-axis) of septin distribution relative to the polar cap (x-axis). Lines are smoothed representations of time-averaged data (37 time points; 20min intervals for 12hrs) and shaded regions surrounding lines are 95% confidence intervals. Lines are representative of two combined experiments (*gpa1*^{G302S}-*rga1Δ* n = 79 cells, *gpa1*^{G302S}-*rga2Δ* n = 80 cells, and *gpa1*^{G302S}-*bem3Δ* n = 87 cells).

Figure 4. Gα control of septins can be mediated by either of the endocytic adaptor proteins, Ent1 or Ent2.

A) Schematic representation of our predicted outcome for individual genetic deletion of Ent1 or Ent2 in *gpa1*^{G302S} yeast. We predicted the lack of either Ent1 or Ent2 would reduce septin recruitment to sites of polarity during the pheromone response and ultimately rescue the *gpa1*^{G302S} phenotype of early septin deposition (top-panel). B) Representative images of pheromone treated yeast (2hrs with saturating pheromone) expressing endogenous Bem1-GFP (Polar Cap) and Cdc3-mCherry (Septin) in *gpa1*^{G302S} cells lacking Ent1 (middle-panels) and in *gpa1*^{G302S} cells lacking Ent2 (bottom-panels). Scale bar represents 3µm and white arrows indicate sites of peripheral septin localization. C) Representative images of *gpa1*^{G302S}*-ent1Δ* cells expressing endogenous Bem1-GFP (Polar Cap) and Cdc3-mCherry (Septin) exposed to saturating pheromone in a microfluidic chamber for 12hrs. Images of cells at 0min (top row), 360min (middle-row), and 720min (bottom row) are displayed with split-channel (left and middle columns) and merged images (right column). Scale bar represents 5µm. D) Representative images of *gpa1*^{G302S}*-ent2Δ* yeast expressing endogenous Bem1-GFP (Polar Cap) and Cdc3-mCherry (Septin) exposed to saturating pheromone in a microfluidic chamber for 12hrs. Images of cells at 0min (top row), 360min (middle-row), and 720min (bottom row) are displayed with split-channel (left and middle columns) and merged images (right column). Scale bar represents 5µm. E) Time-averaged quantification of the fraction (y-axis) of septin distribution relative to the polar cap (x-axis). Lines are smoothed representations of time-averaged data (37 time points; 20min intervals for 12hrs) and shaded regions surrounding lines are 95% confidence intervals.

Lines are representative of two combined experiments (*gpa1*^{G302S}-*ent1Δ* n = 92 cells and *gpa1*^{G302S}-*ent2Δ* n = 55 cells).

Figure 5. A stochastic agent-based model of protein trafficking.

Schematic representation of the mathematical model of protein trafficking in which, (A) naïve cargo (unmodified) is first phosphorylated, then ubiquitinated. Upon ubiquitination, the cargo is considered “endocytically competent”. (B) The plasma membrane is represented by a 1-dimensional line segmented using 100 initial bins. Bins are removed via endocytosis and new bins are added via exocytosis. (C) The location of exocytosis is restricted to the center of the membrane with the given probability distribution. (D) In contrast, the location of endocytosis depends on two factors: location of endocytic pit formation and endocytic pit maturity. Endocytic pits form at sites with a high concentration of endocytosis competent cargo. Endocytic pits cannot diffuse, but their relative position on the membrane changes as bins are added and removed by vesicle trafficking. (E) To determine the directionality of cargo diffusion we employed an agent-based probability model. Briefly, the probability a cargo will diffuse to a bin is inversely correlated with how much cargo is currently in that bin. (F) Finally, once a ubiquitinated cargo enters an endocytic pit, it can no longer diffuse, leading to accumulation of endocytic cargo.

Figure 6. Simulations of cargo becoming competent for endocytosis at higher rates move endocytic events closer to the polar cap.

To change endocytic competency rate, we modified the phosphorylation probability 1-, 5-, and 25-fold. (A) Kymographs from individual simulations showing all cargo on the membrane over time. (B) Kymographs from individual simulations showing ubiquitinated cargo on the membrane over time. (C) Histograms of the location of endocytic events for 11 independent simulations per phosphorylation probability (1-, 5-, and 25-fold). 1X phosphorylation rate yields a distribution of endocytic events that mirrors WT septin localization. While increased phosphorylation probabilities (5-fold and 25-fold higher) result in endocytic events occurring closer to the site of polarity.

Figure 7. Computational modelling predicts that endocytic cargo dynamics are capable of generating septin distribution patterns.

Comparisons of model-generated simulations of the distribution of endocytic events with experimentally determined septin distributions. All plots have been normalized to have a maximum value of 1. A) Comparison of the low (1x phosphorylation) and high (25x phosphorylation) rates of endocytosis competency from Figure 6 with the WT and *gpa1*^{G302S} septin distributions in 300 nM pheromone from Figure 1. B) The model suggests that a higher rate of endocytosis competency would push endocytic events closer to the center of the polar cap (on the left). Since we hypothesize that rate of endocytosis competency is influenced by Gpa1 activity levels, we added a high level of pheromone (10 µM) and measured septin distribution (right). Shaded area represents 95% confidence intervals, n = 293 cells across two independent experiments.

Figure 8. Gα control of septin deposition is driven by its ubiquitination domain

(A) Schematic representation of our predicted outcome for genetic deletion of the receptor C-terminus or the ubiquitin domain (UD) of Gα – both domains are required for the endocytosis of either protein – in *gpa1*^{G302S} mutant yeast. We predicted that cells lacking the capacity to drive endocytosis of either the receptor, Ste2, or the Gα, Gpa1, would reduce septin recruitment to sites of polarity during the pheromone response and ultimately rescue the *gpa1*^{G302S} phenotype of early septin deposition (top-panel). B) Representative images of pheromone treated yeast (2hrs with saturating pheromone) expressing endogenous Bem1-GFP (Polar Cap) and Cdc3-mCherry (Septin) in *gpa1*^{G302S} cells lacking the receptor C-terminus (*gpa1*^{G302S}-*ste2*$^{\Delta C}$) (middle-panels) and in *gpa1*^{G302S} cells lacking the UD of Gα (*gpa1*$^{G302S\text{-}\Delta UD}$) (bottom-panels). Scale bar represents 3µm. (C) Representative images of *gpa1*^{G302S}-*ste2*$^{\Delta C}$ cells expressing endogenous Bem1-GFP (Polar Cap) and Cdc3-mCherry (Septin) exposed to saturating pheromone in a microfluidic chamber for 12hrs. Images of cells at 0min (top row), 360min (middle-row), and 720min (bottom row) are displayed with split-channel (left and middle columns) and merged images (right column). Arrows show sites of septin organization coincident with the polar cap. Scale bar represents 5µm. (D) Representative images of *gpa1*$^{G302S\text{-}UD\Delta}$ yeast expressing endogenous Bem1-GFP (Polar Cap) and Cdc3-mCherry (Septin) exposed to saturating pheromone in a microfluidic chamber for 12hrs. Images of cells at 0min (top row), 360min (middle row), and 720min (bottom row) are displayed with split-channel (left and middle columns) and merged images (right column). Scale bar represents 5µm. (E) Time-averaged quantification of the fraction (y-axis) of septin distribution relative to the polar cap (x-

axis). Lines are smoothed representations of time-averaged data (37 time points; 20min intervals for 12hrs) and shaded regions surrounding lines are 95% confidence intervals. Lines are representative of two combined experiments (*gpa1*^{G302S}-*ste2*$^{\Delta C}$ n = 58 cells and *gpa1*$^{G302S\text{-}\Delta UD}$ n = 93 cells).

Figure 9. Diagram of proposed mechanism. A) Proposed molecular mechanism for three scenarios: 1) The Gpa1 independent pathway, which would use Gics and Cdc42-GAPs to promote septin organization, similar to mitotic processes. 2) The standard Gpa1-regulated pathway, where we propose Gpa1 recruits epsins and Cdc42-GAPs to sites of high Gpa1 activity, leading to septin organization. and 3) The Hyperactive Gpa1 scenario, where Gpa1 activity is high close to the center of the polar cap, leading to faster recruitment of endocytic machinery, and therefore septin organization closer to the center of the polar cap than normal. Consistent with our mathematical modeling, proteins that stay on the membrane longer also travel further from the polar cap, thus faster recruitment of endocytic adaptors leads to less distance traveled. The diagram fades to the left to indicate that this is a symmetric process that we are showing only one side of. B) Proposed mechanism for the asymmetric distribution of septins during gradient tracking. Note that delivery of vesicles to the center of the polarity site and removal distal to the polarity site creates a “treadmill” effect where plasma membrane moves away from the center and towards the sites of endocytosis. On the left, when the polar cap (where exocytosis is occurring) is oriented towards the source of pheromone, the amount of signal to either side of the polar cap is equal, Gpa1 activation levels are similar, leading to similar amounts of endocytosis, and symmetric septin organization. On the right, the polarity site (where exocytosis is occurring) is not oriented towards the source of pheromone, instead high pheromone to the right of the polarity site is driving increased endocytosis relative to the opposite side of the polarity site, leading to asymmetric distribution of septins.

Reference List

Aguilar, R.C., S.A. Longhi, J.D. Shaw, L.-Y. Yeh, S. Kim, A. Schön, E. Freire, A. Hsu, W.K. McCormick, and H.A. Watson. 2006. Epsin N-terminal homology domains perform an essential function regulating Cdc42 through binding Cdc42 GTPase-activating proteins. *Proceedings of the National Academy of Sciences*. 103:4116-4121.

Alvaro, C.G., and J. Thorner. 2016. Heterotrimeric G Protein-coupled Receptor Signaling in Yeast Mating Pheromone Response. *The Journal of biological chemistry*. 291:7788-7795.

Apanovitch, D.M., K.C. Slep, P.B. Sigler, and H.G. Dohlman. 1998. Sst2 is a GTPase-activating protein for Gpa1: purification and characterization of a cognate RGS-Galpha protein pair in yeast. *Biochemistry*. 37:4815-4822.

Azimi, M., Y. Jamali, and M.R. Mofrad. 2011. Accounting for diffusion in agent based models of reaction-diffusion systems with application to cytoskeletal diffusion. *PLoS One*. 6:e25306.

Bennet, M.A., P.R. Richardson, J. Arlt, A. McCarthy, G.S. Buller, and A.C. Jones. 2011. Optically trapped microsensors for microfluidic temperature measurement by fluorescence lifetime imaging microscopy. *Lab on a Chip*. 11:3821-3828.

Bharucha, J.P., J.R. Larson, J.B. Konopka, and K. Tatchell. 2008. Saccharomyces cerevisiae Afr1 protein is a protein phosphatase 1/Glc7-targeting subunit that regulates the septin cytoskeleton during mating. *Eukaryot Cell*. 7:1246-1255.

Brennwald, P. 2013. Membrane traffic: the exocyst meets the cell cycle. *Current biology : CB*. 23:R838-840.

Bridges, A.A., and A.S. Gladfelter. 2015. Septin Form and Function at the Cell Cortex. *The Journal of biological chemistry*. 290:17173-17180.

Burke, D., D. Dawson, and T. Stearns. 2000. Methods in yeast genetics: a Cold Spring Harbor Laboratory course manual (2000 edition). *Plainview, NY: Cold Spring Harbor Laboratory Press.[Google Scholar]*.

Carrillo, L., B. Cucu, V. Bandmann, U. Homann, B. Hertel, S. Hillmer, G. Thiel, and A. Bertl. 2015. High-resolution membrane capacitance measurements for studying endocytosis and exocytosis in yeast. *Traffic*. 16:760-772.

Changwei, Z., X. Mingyong, and W. Ranran. 2007. Afr1p has a role in regulating the localization of Mpk1p at the shmoo tip inSaccharomyces cerevisiae. *FEBS Letters*. 581:2670-2674.

Chee, M.K., and S.B. Haase. 2012. New and redesigned pRS plasmid shuttle vectors for genetic manipulation of Saccharomyces cerevisiae. *G3: Genes| Genomes| Genetics*. 2:515-526.

Chen, H., S. Fre, V.I. Slepnev, M.R. Capua, K. Takei, M.H. Butler, P.P. Di Fiore, and P. De Camilli. 1998. Epsin is an EH-domain-binding protein implicated in clathrin-mediated endocytosis. *Nature*. 394:793-797.

Coon, B.G., J. Burgner, J.H. Camonis, and R.C. Aguilar. 2010. The epsin family of endocytic adaptors promotes fibrosarcoma migration and invasion. *J Biol Chem*. 285:33073-33081.

de Godoy, L.M., J.V. Olsen, J. Cox, M.L. Nielsen, N.C. Hubner, F. Frohlich, T.C. Walther, and M. Mann. 2008. Comprehensive mass-spectrometry-based proteome quantification of haploid versus diploid yeast. *Nature*. 455:1251-1254.

DiBello, P.R., T.R. Garrison, D.M. Apanovitch, G. Hoffman, D.J. Shuey, K. Mason, M.I. Cockett, and H.G. Dohlman. 1998. Selective uncoupling of RGS action by a single point mutation in the G protein alpha-subunit. *The Journal of biological chemistry*. 273:5780-5784.

Dixit, G., R. Baker, C.M. Sacks, M.P. Torres, and H.G. Dohlman. 2014a. Guanine Nucleotide-binding Protein (Gα) Endocytosis by a Cascade of Ubiquitin Binding Domain Proteins Is Required for Sustained Morphogenesis and Proper Mating in Yeast. *Journal of Biological Chemistry*. 289:15052-15063.

Dixit, G., J.B. Kelley, J.R. Houser, T.C. Elston, and H.G. Dohlman. 2014b. Cellular noise suppression by the regulator of G protein signaling Sst2. *Molecular cell*. 55:85-96.

Dohlman, H.G., J. Song, D. Ma, W.E. Courchesne, and J. Thorner. 1996. Sst2, a negative regulator of pheromone signaling in the yeast Saccharomyces cerevisiae: expression, localization, and genetic interaction and physical association with Gpa1 (the G-protein alpha subunit). *Molecular and cellular biology*. 16:5194-5209.

Dores, M.R., J.D. Schnell, L. Maldonado-Baez, B. Wendland, and L. Hicke. 2010. The function of yeast epsin and Ede1 ubiquitin-binding domains during receptor internalization. *Traffic*. 11:151-160.

Dunn, R., and L. Hicke. 2001. Domains of the Rsp5 ubiquitin-protein ligase required for receptor-mediated and fluid-phase endocytosis. *Mol Biol Cell*. 12:421-435.

Giot, L., and J. Konopka. 1997. Functional analysis of the interaction between Afr1p and the Cdc12p septin, two proteins involved in pheromone-induced morphogenesis. *Mol Biol Cell*. 8:987-998.

Gladfelter, A.S., I. Bose, T.R. Zyla, E.S. Bardes, and D.J. Lew. 2002. Septin ring assembly involves cycles of GTP loading and hydrolysis by Cdc42p. *J Cell Biol*. 156:315-326.

Gladfelter, A.S., L. Kozubowski, T.R. Zyla, and D.J. Lew. 2005. Interplay between septin organization, cell cycle and cell shape in yeast. *J Cell Sci*. 118:1617-1628.

Hicke, L., and H. Riezman. 1996. Ubiquitination of a yeast plasma membrane receptor signals its ligand-stimulated endocytosis. *Cell*. 84:277-287.

Hicke, L., B. Zanolari, and H. Riezman. 1998. Cytoplasmic tail phosphorylation of the alpha-factor receptor is required for its ubiquitination and internalization. *The Journal of cell biology*. 141:349-358.

Huh, W.-K., J.V. Falvo, L.C. Gerke, A.S. Carroll, R.W. Howson, J.S. Weissman, and E.K. O'Shea. 2003. Global analysis of protein localization in budding yeast. *Nature*. 425:686-691.

Iwase, M., J. Luo, S. Nagaraj, M. Longtine, H.B. Kim, B.K. Haarer, C. Caruso, Z. Tong, J.R. Pringle, and E. Bi. 2006. Role of a Cdc42p effector pathway in recruitment of the yeast septins to the presumptive bud site. *Mol Biol Cell*. 17:1110-1125.

Kelley, J.B., G. Dixit, J.B. Sheetz, S.P. Venkatapurapu, T.C. Elston, and H.G. Dohlman. 2015. RGS proteins and septins cooperate to promote chemotropism by regulating polar cap mobility. *Current Biology*. 25:275-285.

Khan, A., M. McQuilken, and A.S. Gladfelter. 2015. Septins and Generation of Asymmetries in Fungal Cells. *Annu Rev Microbiol*. 69:487-503.

Konopka, J.B., D.D. Jenness, and L.H. Hartwell. 1988. The C-terminus of the S. cerevisiae α-pheromone receptor mediates an adaptive response to pheromone. *Cell*. 54:609-620.

Layton, A.T., N.S. Savage, A.S. Howell, S.Y. Carroll, D.G. Drubin, and D.J. Lew. 2011. Modeling vesicle traffic reveals unexpected consequences for Cdc42p-mediated polarity establishment. *Current biology : CB*. 21:184-194.

Longtine, M., H. Fares, and J. Pringle. 1998. Role of the yeast Gin4p protein kinase in septin assembly and the relationship between septin assembly and septin function. *The Journal of cell biology*. 143:719-736.

Lu, R., D.G. Drubin, and Y. Sun. 2016. Clathrin-mediated endocytosis in budding yeast at a glance. *J Cell Sci*. 129:1531-1536.

Marco, E., R. Wedlich-Soldner, R. Li, S.J. Altschuler, and L.F. Wu. 2007. Endocytosis optimizes the dynamic localization of membrane proteins that regulate cortical polarity. *Cell*. 129:411-422.

Matheos, D., M. Metodiev, E. Muller, D. Stone, and M.D. Rose. 2004. Pheromone-induced polarization is dependent on the Fus3p MAPK acting through the formin Bni1p. *The Journal of cell biology*. 165:99-109.

McMurray, M., A. Bertin, G. rd, L. Lam, E. Nogales, and J. Thorner. 2011. Septin filament formation is essential in budding yeast. *Developmental cell*. 20:540-549.

Metodiev, M.V., D. Matheos, M.D. Rose, and D.E. Stone. 2002. Regulation of MAPK function by direct interaction with the mating-specific Gα in yeast. *Science*. 296:1483-1486.

Mukherjee, D., B.G. Coon, D.F. Edwards, C.B. Hanna, S.A. Longhi, J.M. McCaffery, B. Wendland, L.A. Retegui, E. Bi, and R.C. Aguilar. 2009. The yeast endocytic protein Epsin 2 functions in a cell-division signaling pathway. *Journal of Cell Science*. 122:2453-2463.

Okada, S., M. Leda, J. Hanna, N.S. Savage, E. Bi, and A.B. Goryachev. 2013. Daughter cell identity emerges from the interplay of Cdc42, septins, and exocytosis. *Dev Cell*. 26:148-161.

Pedersen, R.T.A., J.E. Hassinger, P. Marchando, and D.G. Drubin. 2020. Spatial regulation of clathrin-mediated endocytosis through position-dependent site maturation. *J Cell Biol*. 219.

Pryciak, P.M., and F.A. Huntress. 1998. Membrane recruitment of the kinase cascade scaffold protein Ste5 by the Gbetagamma complex underlies activation of the yeast pheromone response pathway. *Genes Dev*. 12:2684-2697.

Sadian, Y., C. Gatsogiannis, C. Patasi, O. Hofnagel, R.S. Goody, M. Farkašovský, and S. Raunser. 2013. The role of Cdc42 and Gic1 in the regulation of septin filament formation and dissociation. *Elife*. 2:e01085.

Segall, J.E. 1993. Polarization of yeast cells in spatial gradients of alpha mating factor. *Proceedings of the National Academy of Sciences*. 90:8332-8336.

Shenoy, S.K., and R.J. Lefkowitz. 2003. Multifaceted roles of beta-arrestins in the regulation of seven-membrane-spanning receptor trafficking and signalling. *Biochem J*. 375:503-515.

Simke, W.C., C.P. Johnson, A.J. Hart, S. Mayhue, P.L. Craig, S. Sojka, and J.B. Kelley. 2022. Phosphorylation of RGS regulates MAP kinase localization and promotes completion of cytokinesis. *Life Sci Alliance*. 5.

Slessareva, J., and H. Dohlman. 2006. G protein signaling in yeast: new components, new connections, new compartments. *Science (New York, N.Y.)*. 314:1412-1413.

Smith, G.R., S.A. Givan, P. Cullen, and G.F. Sprague, Jr. 2002. GTPase-activating proteins for Cdc42. *Eukaryot Cell*. 1:469-480.

Smith, J.S., T.F. Pack, A. Inoue, C. Lee, K. Zheng, I. Choi, D.S. Eiger, A. Warman, X. Xiong, Z. Ma, G. Viswanathan, I.M. Levitan, L.K. Rochelle, D.P. Staus, J.C. Snyder, A.W. Kahsai, M.G. Caron, and S. Rajagopal. 2021. Noncanonical scaffolding of G(alphai) and beta-arrestin by G protein-coupled receptors. *Science*. 371.

Spiliotis, E.T., and M.A. McMurray. 2020. Masters of asymmetry - lessons and perspectives from 50 years of septins. *Mol Biol Cell*. 31:2289-2297.

Suzuki, S.K., J.B. Kelley, T.C. Elston, and H.G. Dohlman. 2021. Gradient tracking by yeast GPCRs in a microfluidics chamber. *In* G Protein-Coupled Receptor Screening Assays. Springer. 275-287.

Valdez-Taubas, J., and H. Pelham. 2003. Slow diffusion of proteins in the yeast plasma membrane allows polarity to be maintained by endocytic cycling. *Current biology : CB*. 13:1636-1640.

Wang, Y., L.A. Marotti, Jr., M.J. Lee, and H.G. Dohlman. 2005a. Differential Regulation of G Protein α Subunit Trafficking by Mono- and Polyubiquitination *. *Journal of Biological Chemistry*. 280:284-291.

Wang, Y., L.A. Marotti, Jr., M.J. Lee, and H.G. Dohlman. 2005b. Differential regulation of G protein alpha subunit trafficking by mono- and polyubiquitination. *The Journal of biological chemistry*. 280:284-291.

Wendland, B. 2002. Epsins: adaptors in endocytosis? *Nat Rev Mol Cell Biol*. 3:971-977.

Figure 1

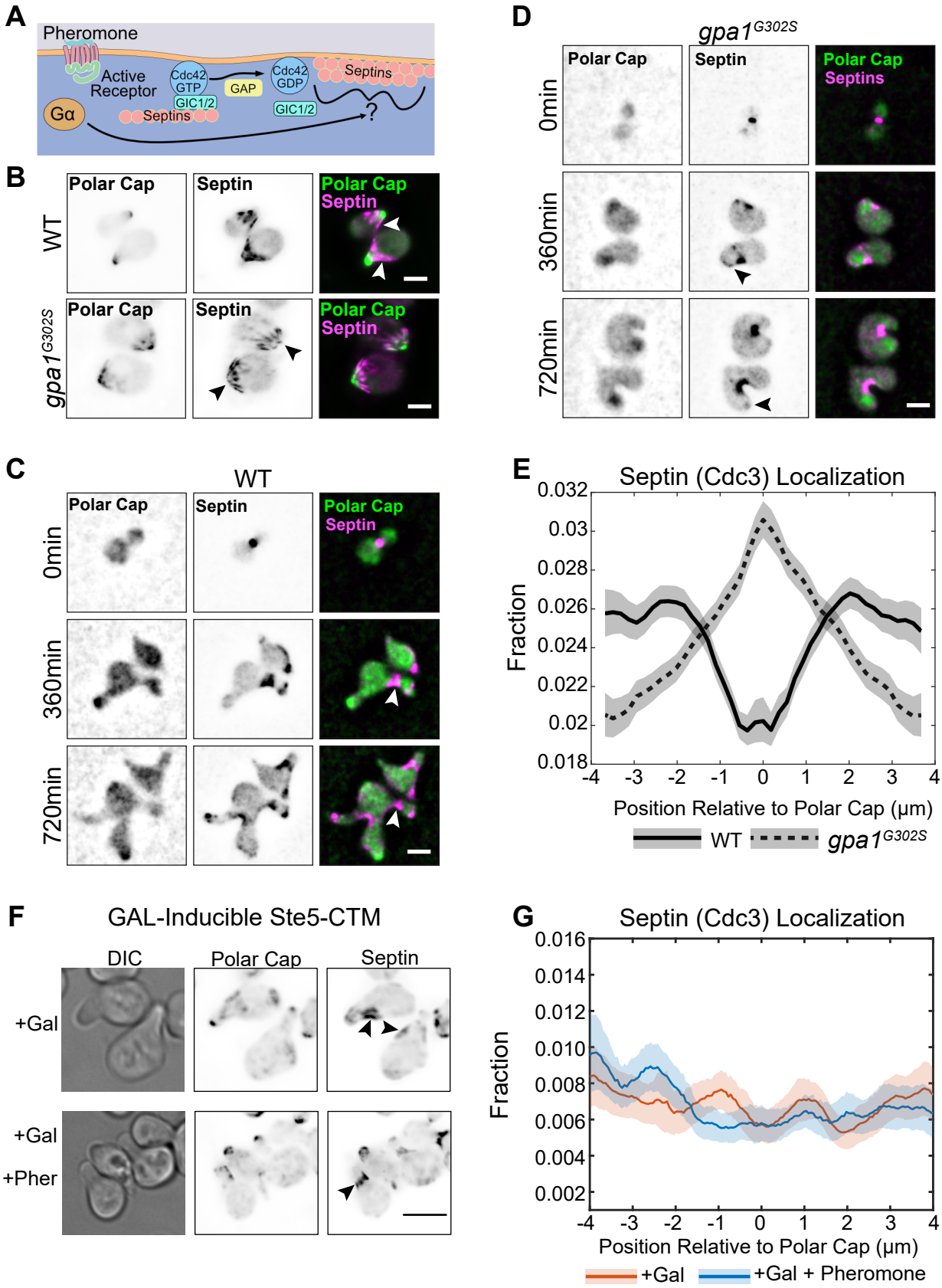
A
Pheromone
Active Receptor
Cdc42 GTP
GAP
Cdc42 GDP
Septins
GIC1/2
Gα
?
B
Polar Cap
Septin
Polar Cap Septin
WT
gpa1G302S
C
WT
0min
360min
720min
D
gpa1G302S
Polar Cap Septins
E
Septin (Cdc3) Localization
Fraction
Position Relative to Polar Cap (μm)
WT
gpa1G302S
F
GAL-Inducible Ste5-CTM
DIC
+Gal
+Pher
G
Septin (Cdc3) Localization
+Gal
+Gal + Pheromone

Figure 2

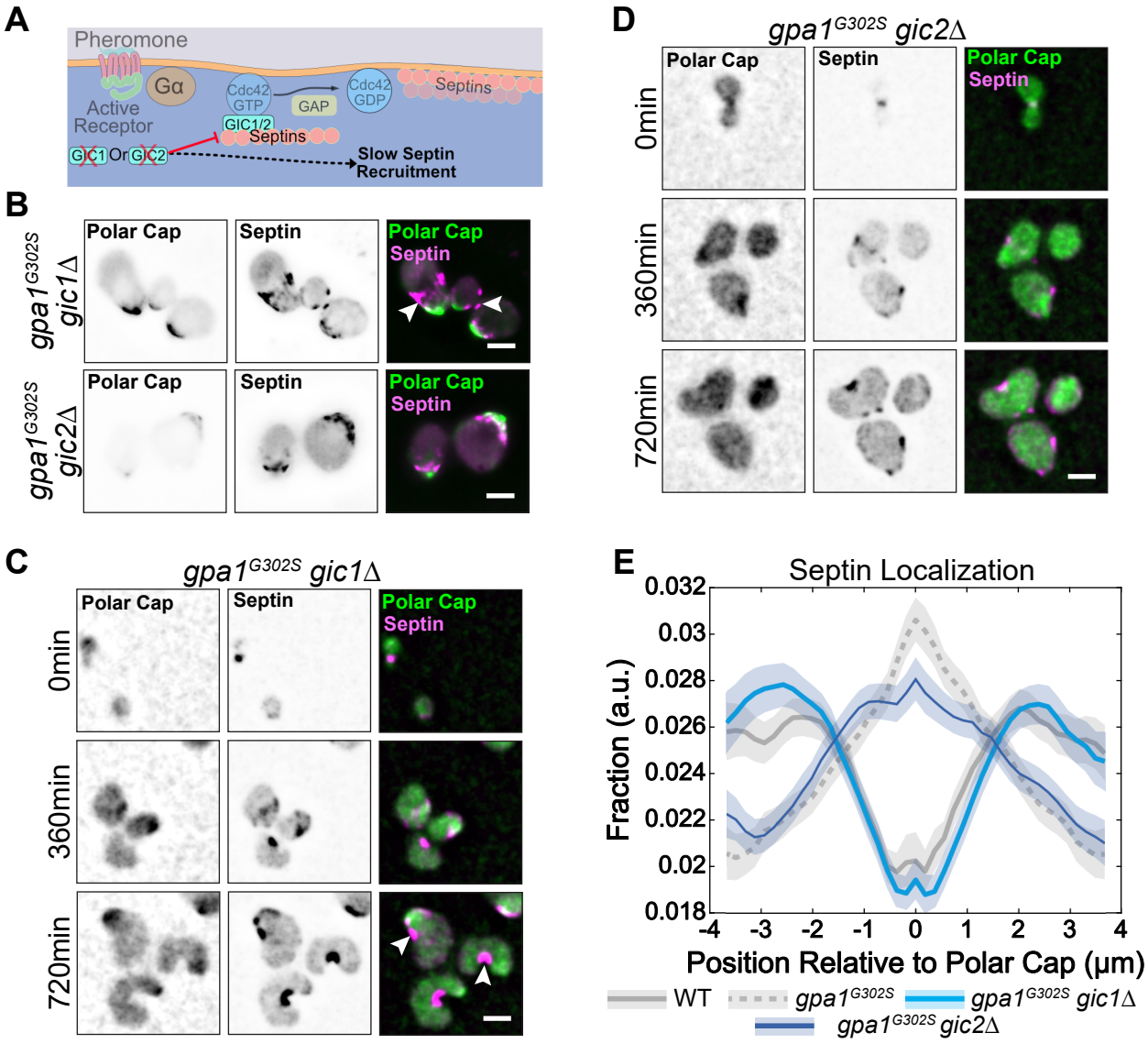
A
Pheromone
Active Receptor
Gα
Cdc42 GTP
GAP
Cdc42 GDP
Septins
GIC1/2
Septins
GIC1 Or GIC2
Slow Septin Recruitment
B
gpa1G302S gic1Δ
gpa1G302S gic2Δ
Polar Cap
Septin
Polar Cap Septin
C
gpa1G302S gic1Δ
0min
360min
720min
D
gpa1G302S gic2Δ
E
Septin Localization
Fraction (a.u.)
Position Relative to Polar Cap (μm)
WT
gpa1G302S
gpa1G302S gic1Δ
gpa1G302S gic2Δ

Figure 3

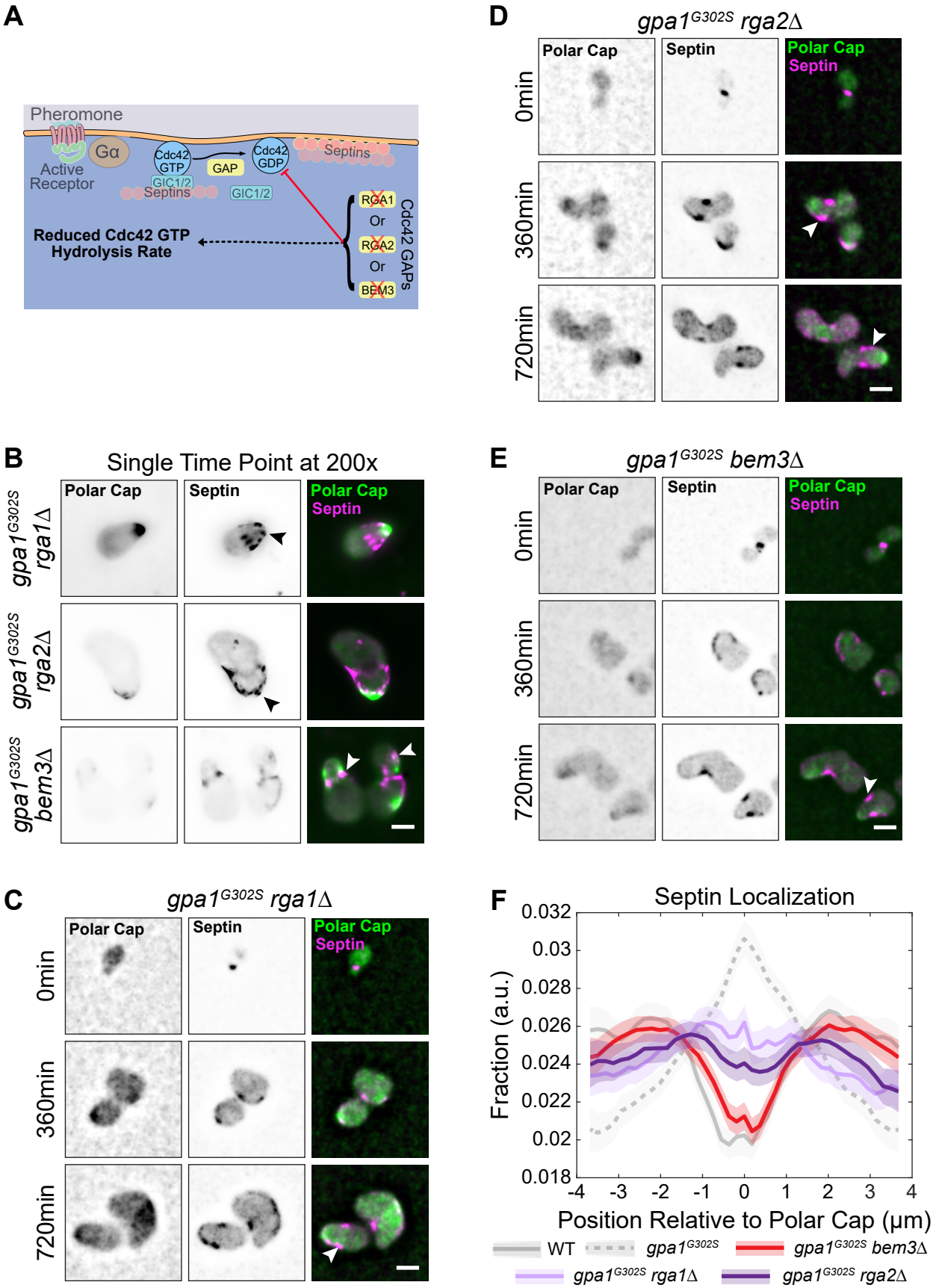
A
Pheromone
Active Receptor
Gα
Cdc42 GTP
GAP
Cdc42 GDP
Septins
GIC1/2
Septins
GIC1/2
RGA1
Or
RGA2
Or
BEM3
Cdc42 GAPs
Reduced Cdc42 GTP Hydrolysis Rate
B
Single Time Point at 200x
gpa1G302S rga1Δ
gpa1G302S rga2Δ
gpa1G302S bem3Δ
Polar Cap
Septin
Polar Cap Septin
C
gpa1G302S rga1Δ
0min
360min
720min
D
gpa1G302S rga2Δ
E
gpa1G302S bem3Δ
F
Septin Localization
Fraction (a.u.)
Position Relative to Polar Cap (μm)
WT
gpa1G302S
gpa1G302S bem3Δ
gpa1G302S rga1Δ
gpa1G302S rga2Δ

Figure 4

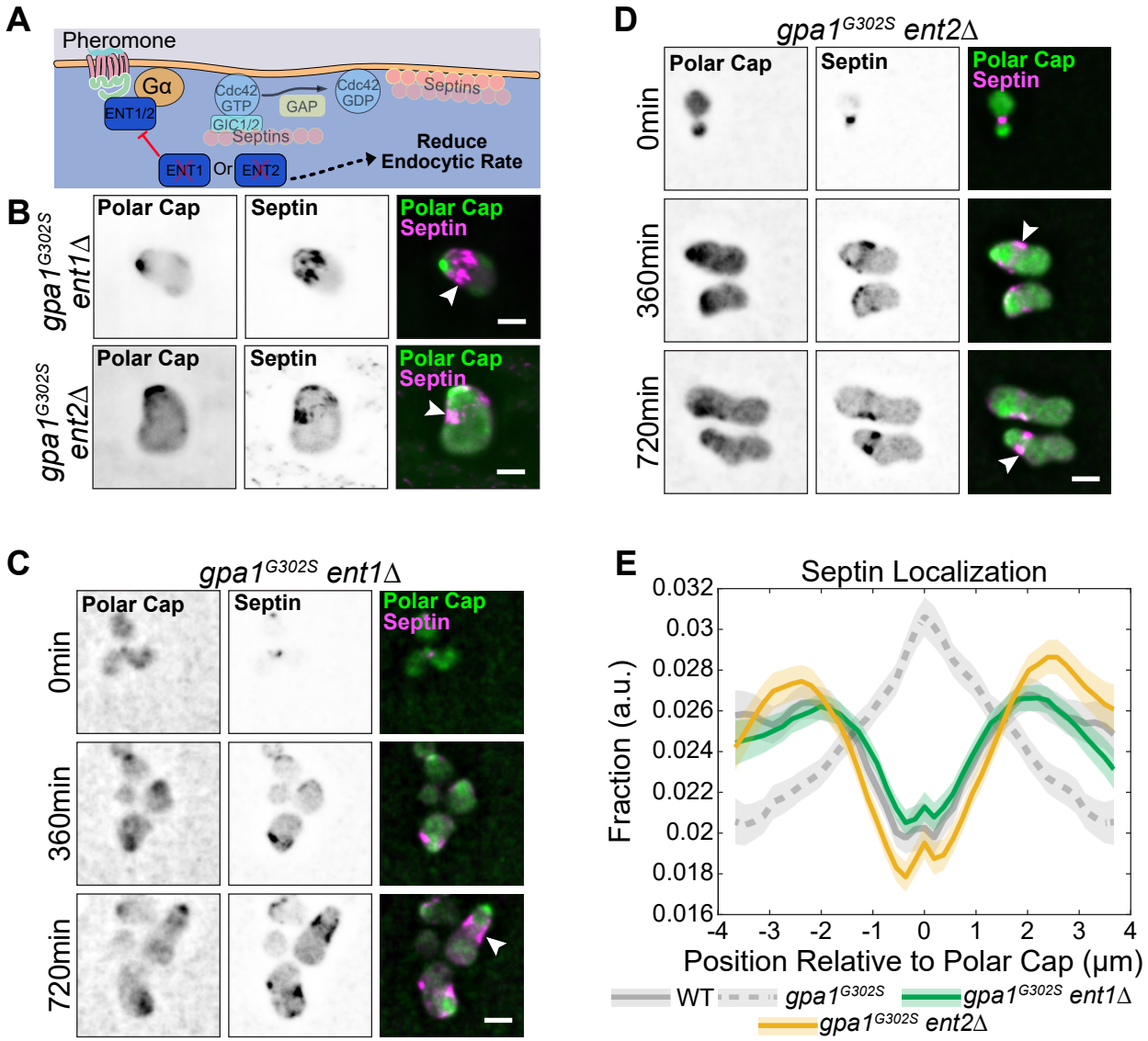
A
Pheromone
Gα
ENT1/2
Cdc42 GTP
GAP
Cdc42 GDP
Septins
GIC1/2
Septins
ENT1
Or
ENT2
Reduce Endocytic Rate
B
gpa1G302S ent1Δ
gpa1G302S ent2Δ
Polar Cap
Septin
Polar Cap Septin
C
gpa1G302S ent1Δ
0min
360min
720min
D
gpa1G302S ent2Δ
E
Septin Localization
Fraction (a.u.)
Position Relative to Polar Cap (μm)
WT
gpa1G302S
gpa1G302S ent1Δ
gpa1G302S ent2Δ

Figure 5

Stochastic Agent-Based Model of Protein Trafficking

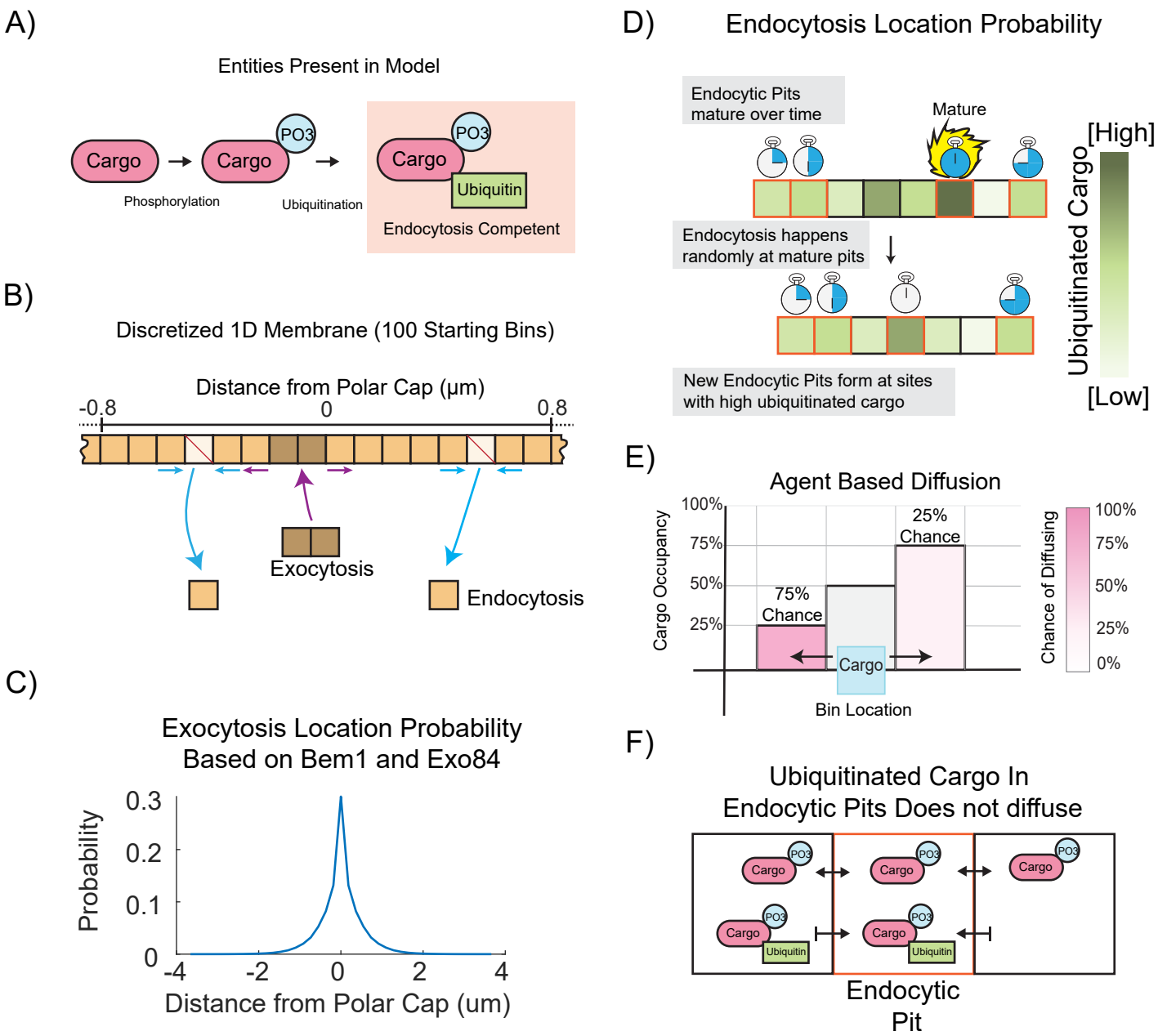

Figure 6

Cargo Simulations

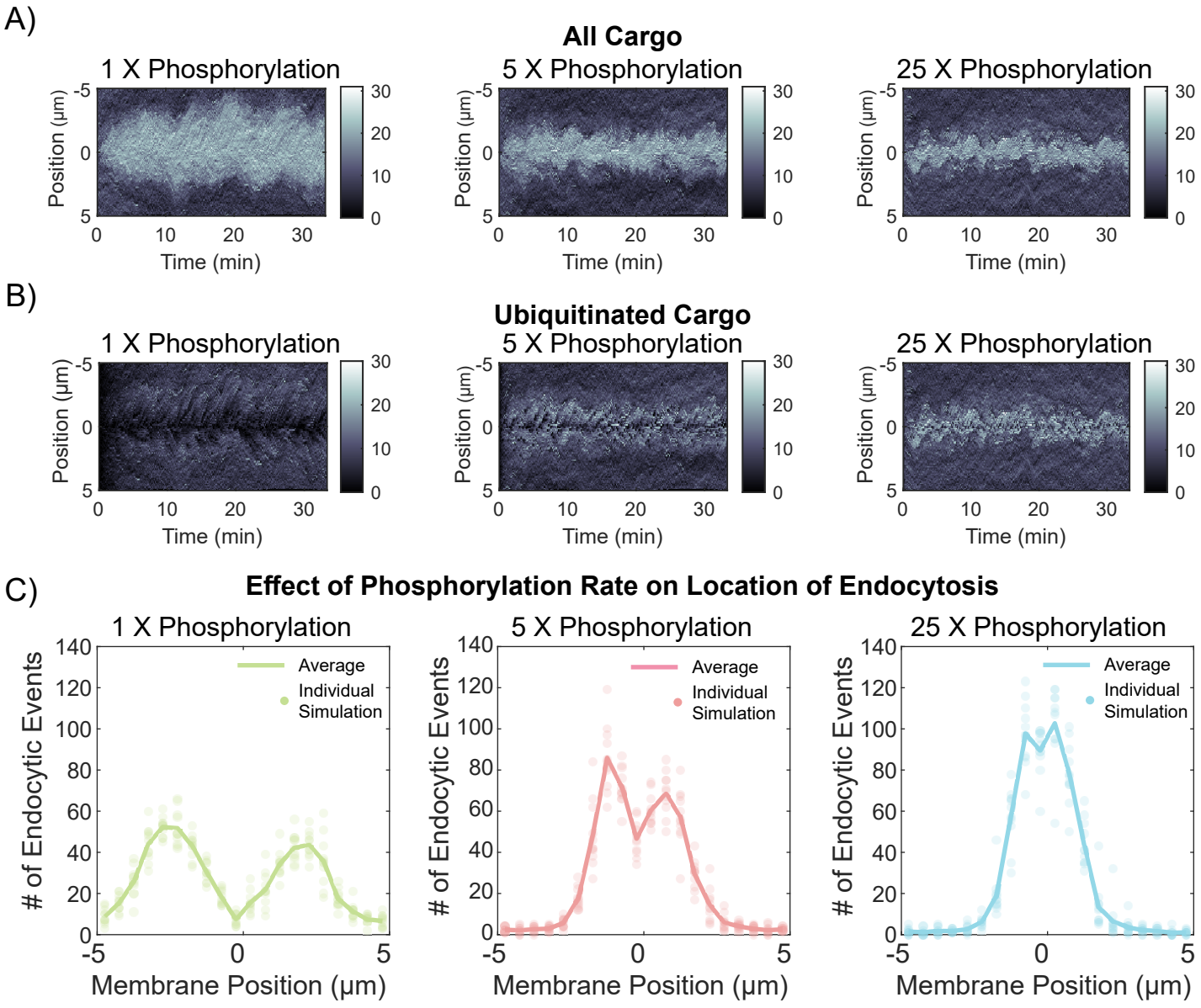

Figure 7

A) Simulations of high and low endocytosis competency rate are able to capture the shape of septin distributions measured in WT and hyperactive Gpa1 at intermediate doses of pheromone

B) Model simulations of an intermediate endocytosis competency rate are able to predict the septin distribution in a high dose of pheromone with a wild-type Gpa1.

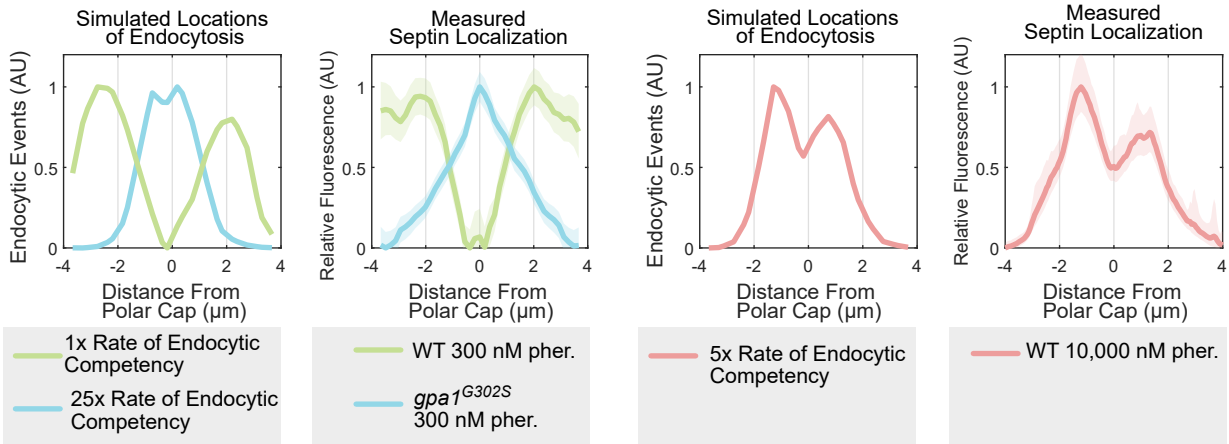

Figure 8

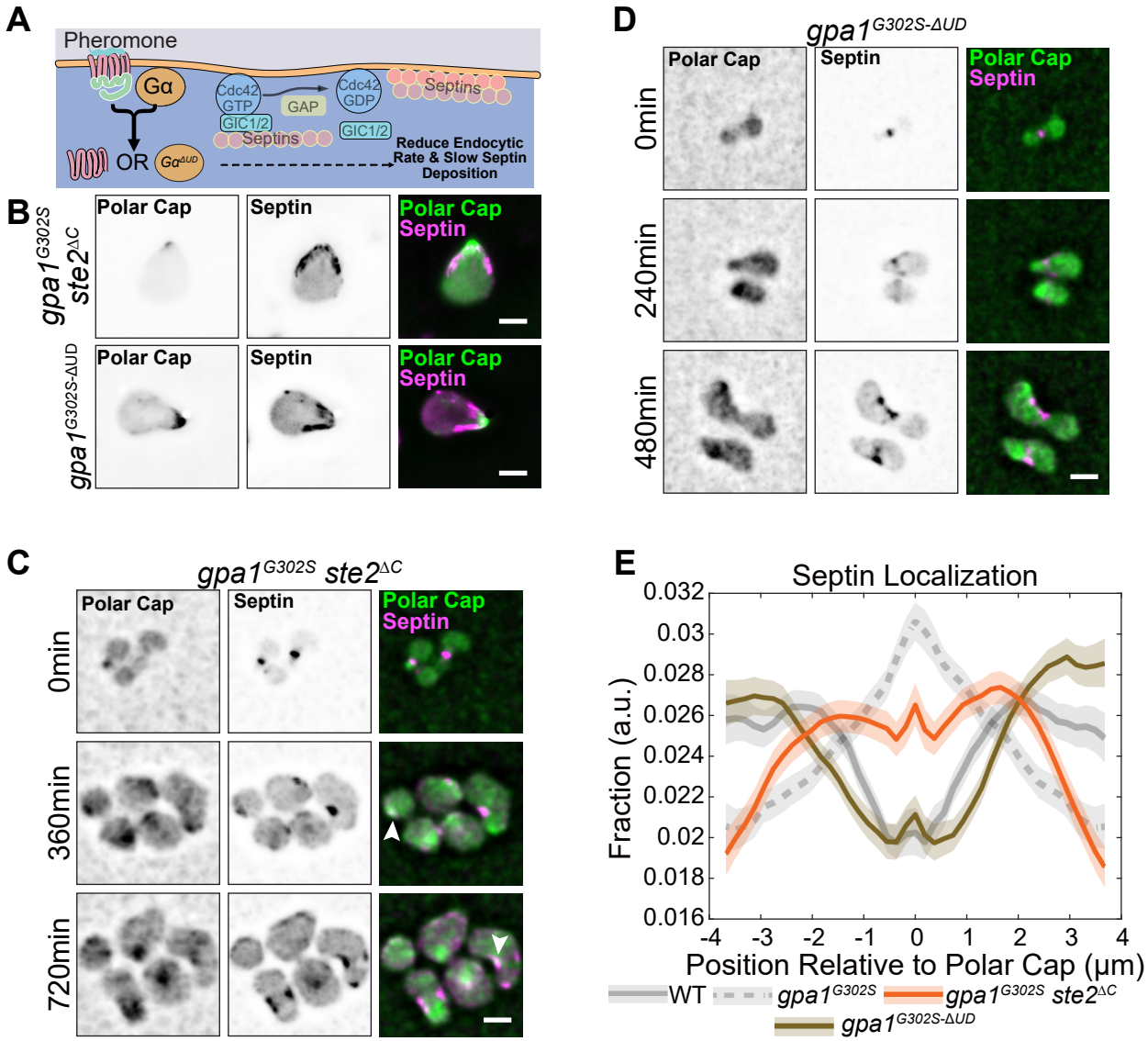
A
Pheromone
Gα
Cdc42 GTP
GAP
Cdc42 GDP
Septins
GIC1/2
Septins
GIC1/2
OR
Gα^ΔUD
Reduce Endocytic Rate & Slow Septin Deposition
B
gpa1^G302S ste2^ΔC
gpa1^G302S-ΔUD
Polar Cap
Septin
Polar Cap Septin
C
gpa1^G302S ste2^ΔC
0min
360min
720min
D
gpa1^G302S-ΔUD
0min
240min
480min
E
Septin Localization
Fraction (a.u.)
Position Relative to Polar Cap (μm)
WT
gpa1^G302S
gpa1^G302S ste2^ΔC
gpa1^G302S-ΔUD

Figure 9

A

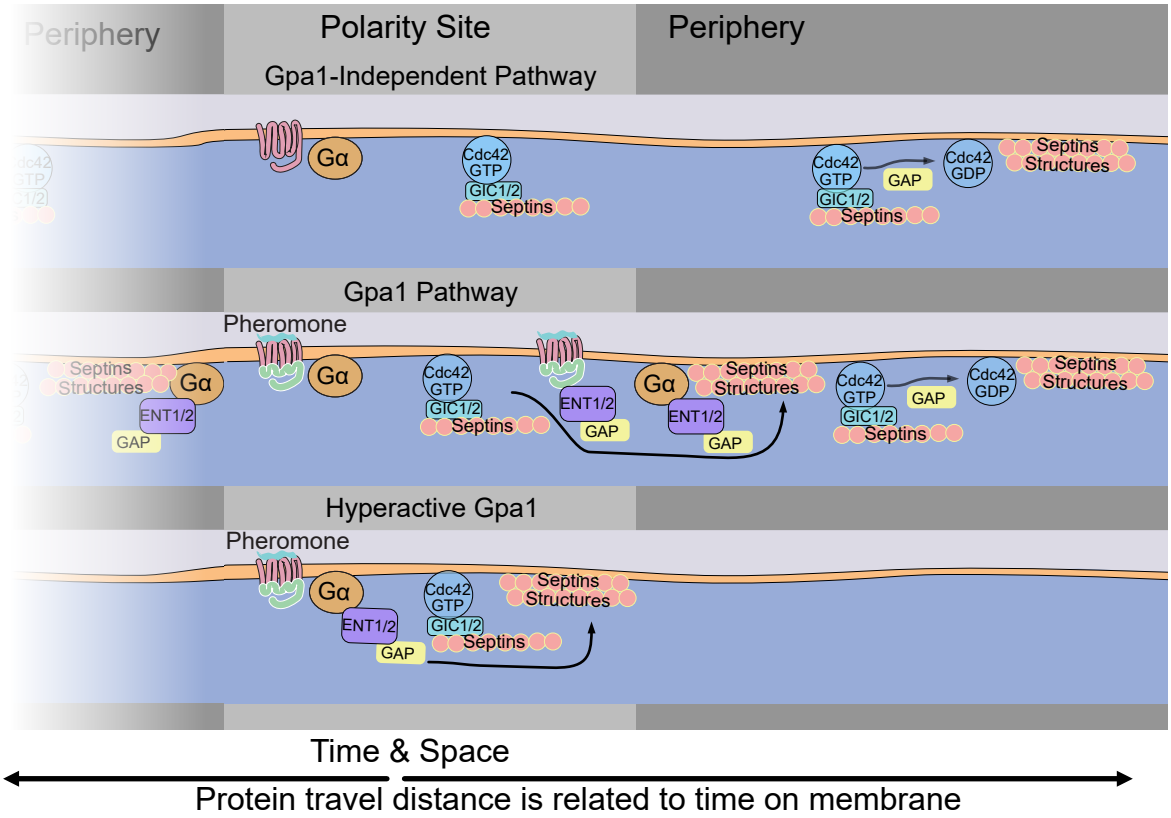

B

Proposed mechanism for asymmetric septin organization

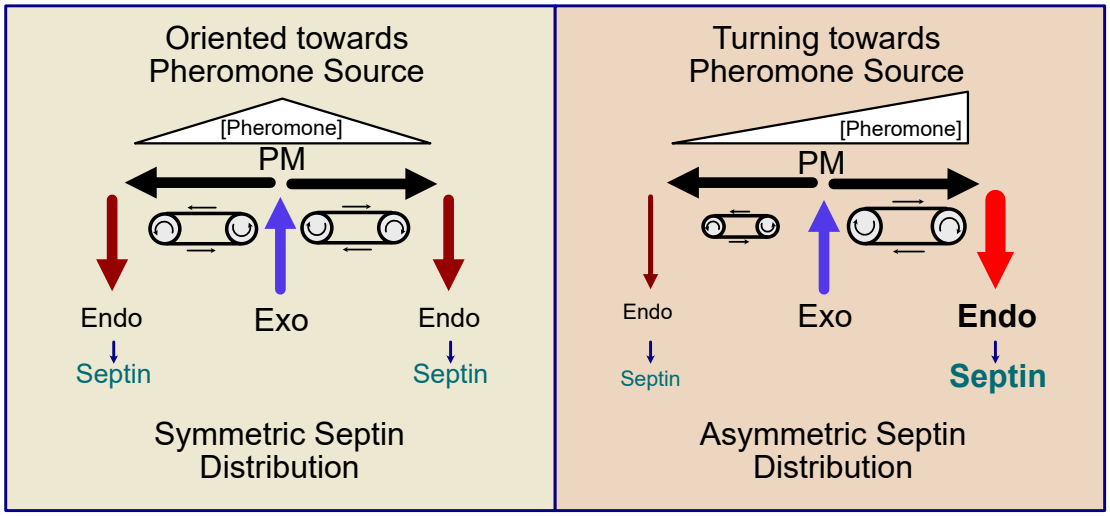

Table 1: Strain List

Strain	***Parent***	***Description***
BEM1-GFP CDC3MCHERRY	BY4741	*BEM1-GFP::HIS3 CDC3MCHERRY::LEU2*
GPA1^{G302S} BEM1-GFP CDC3MCHERRY	BY4741	*gpa1^{G302S}::URA3 BEM1-GFP::HIS3 CDC3MCHERRY::LEU2*
RGA1Δ GPA1^{G302S} BEM1-GFP CDC3MCHERRY	BY4741	*rga1Δ::KanMX4 Gpa1^{G302S}::URA3 BEM1-GFP::HIS3 CDC3MCHERRY::LEU2*
RGA2Δ GPA1^{G302S} BEM1-GFP CDC3MCHERRY	BY4741	*rga2Δ::KanMX4 Gpa1^{G302S}::URA3 BEM1-GFP::HIS3 CDC3MCHERRY::LEU2*
BEM3Δ GPA1^{G302S} BEM1-GFP CDC3MCHERRY	BY4741	*bem3Δ::KanMX4 Gpa1^{G302S}::URA3 BEM1-GFP::HIS3 CDC3MCHERRY::LEU2*
ENT1Δ GPA1^{G302S} BEM1-GFP CDC3MCHERRY	BY4741	*ent1Δ::KanMX4 gpa1^{G302S}::URA3 BEM1-GFP::HIS3 CDC3MCHERRY::LEU2*
ENT2Δ GPA1^{G302S} BEM1-GFP CDC3MCHERRY	BY4741	*ent2Δ::KanMX4 gpa1^{G302S}::URA3 BEM1-GFP::HIS3 CDC3MCHERRY::LEU2*

GIC1Δ GPA1^{G302S} BEM1-GFP CDC3MCHERRY	BY4741	*gic1Δ::KanMX4 Gpa1^{G302S}::URA3 BEM1-GFP::HIS3 CDC3MCHERRY::LEU2*
GIC2Δ GPA1^{G302S} BEM1-GFP CDC3MCHERRY	BY4741	*gic2Δ::KanMX4 Gpa1^{G302S}::URA3 BEM1-GFP::HIS3 CDC3MCHERRY:LEU2*
Ste2^{T326} GPA1^{G302S} BEM1-GFP CDC3MCHERRY	BY4741	*ste2^{T326}::KanMX4 gpa1^{G302S}::URA3 BEM1-GFP::HIS3 CDC3MCHERRY::LEU2*
GPA1$^{G302S\text{-}\Delta UD}$ BEM1-GFP CDC3MCHERRY	BY4741	*gpa1$^{G302S\text{-}\Delta UD}$::URA3 BEM1-GFP::HIS3 CDC3MCHERRY:LEU2*
ENT1-GFP	BY4741	*ENT1-GFP::HIS3*
ENT2-GFP	BY4741	*ENT2-GFP::HIS3*

Table 2: Plasmid List

Plasmid Name	***Vector Backbone***	***Description***
pRSII416-Gpa1-3xFLAG	pRSII416	CEN ADHp-Gpa1-3xFLAG::LEU2 vector
pRSII406-GPA1^{G302S}	pRSII406	Integrating gpa1^{G302S}::URA3 vector
pRSII406-GPA1$^{G302S\text{-}\Delta UD}$	pRSII406	Integrating gpa1$^{G302S\text{-}\Delta UD}$::URA3 vector
pRSII416-GAL-Ste5CTM	pRSII416	Galactose-inducible Ste5-CTM

Table 3: Primer List

Primer Name	***Sequence***	***Description***
AHM-14	5'GGGCCGTATAAAGACTACAGACATTACAGAAACCGAATTTA 3'	Quickchange primer for G302S mutation in Gpa1
AHM-15	5' TAAATTCGGTTTCTGTAATGTCTGTAGTCTTTATAC GGCCC 3'	Quickchange primer for G302S mutation in Gpa1
AHM-44	5' GCGGCCGTTTTATAAAGAACAA 3'	Replicate deletion of Bem3
AHM-45	5' AGAAGTGGTGGAAGATGGTGAT 3'	Replicate deletion of Bem3
AHM-46	5' TTACAGCTTTGCCACATATCGG 3'	Verification of Bem3 del
AHM-47	5' AACAAAACTTTCAATCGCACGG 3'	Verification of Bem3 del
AHM-50	5' GATGAGAAGGTGTAAAGTGCCC 3'	Replicate deletion of Rga1
AHM-51	5' GCCCGTAAAAGGTTCTTGTCTA 3'	Replicate deletion of Rga1
AHM-52	5' AGTGTACCCTTTGAACCCTCTT 3'	Verify Replication of Rga1 del
AHM-53	5' ATCTCTGTCGCTCAAAAGTTGG 3'	Verify Replication of Rga1 del
AHM-54	5' AATCGTTGCATCGCTTCAGTAA 3'	Replicate deletion of Rga2
AHM-55	5' CCGCACAAAAGTACGACAAATG 3'	Replicate deletion of Rga2
AHM-56	5' CTCTGTAGAAGCTTTTCCGGAC 3'	Verify Replication of Rga2 del
AHM-57	5' CTTTACAGAAGTCGCGTCAACT 3'	Verify Replication of Rga2 del

CJM-3	5’ CAATGTGGGCCACGGCTGCTAA 3’	Verify Ste2 C-terminal del
CJM-4	5’ ACAGCGTACCTTTAGACACGTGGG 3’	Verify Ste2 C-terminal del
CJM-5	5’ CATCCACAGATAGGTTTTATCCAGGCACGCT GTCTAGCGTTTAGCTTGCCTCGTCCCCGC 3’	Amplify pFA6-KanMX with Ste2 T-326 homology
CJM-6	5’ AGGTCACGAAATTACTTTTTCAAAGCCGTAA ATTTTGACGTTTAAACTGGATGGCGGCGT 3’	Amplify pFA6-KanMX with Ste2 T-326 homology
SLM-3	5' TAGGCTTCTTACCGGCAGAG 3'	Amplify Ent1 del
SLM-4	5' AGGACATGAGTACAGAGCACA 3'	Amplify Ent1 del
SLM-5	5' AGATAGATGGCCGAACGTGG 3'	Amplify Ent2 del
SLM-6	5' GACTCCAAAGGTGAATCTGGC3'	Amplify Ent2 del
SLM-7	5' GGGAGAAGGAGTACCTTCTG 3'	Verify Ent1 del
SLM-8	5' CCAGAATTATCTTTCGGGCC 3'	Verify Ent1 del
SLM-9	5' ATGGCTCAAATTCCACGGTCC 3'	Verify Ent2 del
SLM-10	5' CGAAGATGGCCGAATGATTGG 3'	Verify Ent2 del
JKM-54	5’ GACTACAAAGACCATGACGGTGATTATAAAGAT CATGACATCGACTACAAGGATGACGATGACAAGTAG 3’	Forward 3X Flag + stop
JKM-55	5’ CTACTTGTCATCGTCATCCTTGTAGTCGATGT CATGATCTTTATAATCACCGTCATGGTCTTTGTAGTC 3’	Reverse 3X Flag + stop
JKM-56	5’ tcgaggtcgacggtatcgatAAGGTGAGACGCGCATAAC 3’	Forward ADH promoter for Gibson assembly of pRSII416-ADHp-Gpa1-3XFlag
JKM-57	5’ tacaccccatTGTATATGAGATAGTTGA	reverse ADH promoter for

	TTGTATGCTTG 3’	Gibson assembly of pRSII416-ADHp-Gpa1-3XFlag
JKM-58	5’ctcatatacaATGGGGTGTACAGTGAGTAC 3’	forward GPA1 for Gibson assembly of pRSII416-ADHp-Gpa1-3XFlag
JKM-59	5’ ctttgtagtcTATAATACCAATTTTTTTAAG GTTTTGCTG 3’	reverse GPA1 for Gibson assembly of pRSII416-ADHp-Gpa1-3XFlag
JKM-60	5’ tggtattataGACTACAAAGACCATGAC 3’	forward 3x Flag for Gibson assembly of pRSII416-ADHp-Gpa1-3XFlag, uses JKM-54 and 55 as template
JKM-61	5’ gcggccgctctagaactagtCTACTTGTCATCGTCATC 3’	reverse 3x Flag for Gibson assembly of pRSII416-ADHp-Gpa1-3XFlag, uses JKM-54 and 55 as template